NASA-CR-159522
19790010902

NASA CR-159522

STRUCTURAL ANALYSIS OF CYLINDRICAL THRUST CHAMBERS FINAL REPORT VOLUME I

CONTRACT NAS3-21361

MARCH 1979

Prepared by

LOCKHEED MISSILES & SPACE COMPANY, INC.
HUNTSVILLE RESEARCH & ENGINEERING CENTER
HUNTSVILLE, ALABAMA

Prepared for

NATIONAL AERONAUTICS & SPACE ADMINISTRATION
LEWIS RESEARCH CENTER
CLEVELAND, OHIO

1. Report No.	2. Government Accession No.	3. Recipient's Catalog No.
NASA CR-159522		

4. Title and Subtitle	5. Report Date
STRUCTURAL ANALYSIS OF CYLINDRICAL THRUST CHAMBERS – FINAL REPORT – VOLUME I	March 1979
	6. Performing Organization Code
7. Author(s)	8. Performing Organization Report No.
W.H. Armstrong	LMSC-HREC TR D568827
	10. Work Unit No.
9. Performing Organization Name and Address	
Lockheed Missiles & Space Company, Inc. Huntsville Research & Engineering Center 4800 Bradford Drive, Huntsville, AL 35807	11. Contract or Grant No. NAS3-21361
	13. Type of Report and Period Covered Final May 1978 to March 1979
12. Sponsoring Agency Name and Address	14. Sponsoring Agency Code
National Aeronautics and Space Administration 2100 Brookpark Road Lewis Research Center Cleveland, OH 44135	

15. Supplementary Notes

H.J. Kasper, NASA Technical Monitor

16. Abstract

Life predictions of regeneratively cooled rocket thrust chambers are normally derived from classical material fatigue principles. The failures observed in experimental thrust chambers do not appear to be due entirely to material fatigue. The chamber coolant walls in the failed areas have exhibited progressive bulging and thinning during cyclic firings until the wall stress finally exceeds the material rupture stress and failure occurs. A preliminary analysis of an oxygen free high conductivity (OFHC) copper cylindrical thrust chamber demonstrated that the inclusion of cumulative cyclic plastic effects enables the observed coolant wall thinout to be predicted. The thinout curve constructed from the referent analysis of 10 firing cycles was extrapolated from the tenth cycle to the 200th cycle. The study contained herein extends the preliminary OFHC copper chamber 10-cycle analysis so that the extrapolated thinout curve could be established by performing cyclic analysis of deformed configurations at 100 and 200 cycles. Thus the original range of extrapolation was reduced and the thinout curve was adjusted by using calculated thinout rates at 100 and 200 cycles. The study also includes an analysis of the same undeformed chamber model constructed of half-hard Amzirc to study the effect of material properties on the thinout curve.

17. Key Words (Suggested by Author(s))	18. Distribution Statement
Thrust Chamber Nonlinear Finite-Element Analysis Finite Deformation	Unclassified – Unlimited

19. Security Classif. (of this report)	20. Security Classif. (of this page)	21. No. of Pages	22. Price*
Unclassified	Unclassified	52	

* For sale by the National Technical Information Service, Springfield, Virginia 22161

N79-19073#

Lockheed
MISSILES
& SPACE
COMPANY,
INC.

HUNTSVILLE RESEARCH & ENGINEERING CENTER • P. O. BOX 1103 • HUNTSVILLE, ALABAMA • 35807

In reply refer to:
LMSC-HREC D568923
22 March 1979

National Aeronautics and Space Administration
2100 Brookpark Road
Lewis Research Center
Cleveland, OH 44135

Attention: J.R. Danicic, 500-313

Subject: Contract NAS3-21361, Submittal of Final Report – Volume I

Gentlemen:

The enclosed report is submitted as the Final Report – Volume I – as required under the subject contract. Your acceptance of this report by return correspondence is requested.

Very truly yours,

LOCKHEED MISSILES & SPACE CO., Inc.

for Ronald R. Gautchen
J.E. Eckert, Contracts
Huntsville Research & Engineering Center

JEE:pgp

Encl: LMSC-HREC TR D568827, "Structural Analysis of Cylindrical Thrust Chambers – Final Report – Volume I.

Distribution:
See back of report.

FOREWORD

This final report was prepared by Lockheed Missiles & Space Company, Inc., Huntsville, Alabama, for Lewis Research Center (LeRC), National Aeronautics and Space Administration, Cleveland, Ohio. The analytical evaluation of finite deformations of rocket engine test chambers subjected to constant amplitude thermomechanical loading cycles was conducted in accordance with requirements of Contract NAS3-21361 "Structural Analysis of Cylindrical Thrust Chambers." The study was under the cognizance of H. J. Kasper of NASA-LeRC.

The analyses and documentation of results were conducted by W. H. Armstrong.

CONTENTS

1. SUMMARY

The objective of this study was to determine analytically the cumulative plastic deformation characteristic of damage observed in coolant channel walls of regeneratively cooled rocket thrust chambers. The damage of the channel wall consists of bulging and plastic flow which leads to thinout and rupture of the channel wall under the high pressures and high temperatures and temperature gradients experienced during successive cyclic firings of the thrust chamber. The study involves the structural analyses of two LeRC test chambers of the same geometric configuration but constructed from different copper alloys.

The applied thermomechanical loading cycle was assumed constant in amplitude and period. Axisymmetric structural temperature and pressure load histories were provided by LeRC.

Structural response to the provided loading cycle was determined with the use of the BOPACE finite element computer program. Generalized plane-strain elements were used to model and analyze quasi three-dimensional behavior of the throat region of the thrust chambers.

Results are presented which show calculated permanent distortions of the chamber walls; nodal displacement plots of the hot gas and coolant surfaces and channel wall thicknesses as functions of number of loading cycles are included.

2. INTRODUCTION

Life predictions of regeneratively cooled rocket thrust chambers are normally derived from classical material fatigue principles. The failures observed in experimental thrust chambers do not appear to be due entirely to material fatigue. The chamber coolant walls in the failed areas have exhibited progressive bulging and thinning during cyclic firings until the wall stress finally exceeds the material rupture stress and failure occurs. This is not to imply that the primary cause of failure is simply a case of applied stress exceeding the material strength in the deformed chamber. The large strains evidenced by plastic flow in the failed areas obviously result in material damage as well as thinout of the coolant wall. The failure mechanism possibly consists of the development of a low cycle fatigue crack which grows rapidly to a critical flaw size in the thinned wall. Consequently, analytically tracing the chamber wall thinout and changes in coolant passage geometry are important factors when attempting to predict thrust chamber life.

A preliminary analysis of an oxygen free high conductivity (OFHC) copper cylindrical thrust chamber (Ref. 1) demonstrated that the inclusion of cumulative cyclic plastic effects enables the observed coolant wall thinout to be predicted. The thinout curve constructed from the referent analysis of 10 firing cycles was extrapolated from the tenth cycle to the 200th cycle. Additional analysis was required to evaluate the extrapolation and study the effects of material properties on the analytical results.

The study contained herein extends the preliminary OFHC copper chamber 10-cycle analysis so that the extrapolated thinout curve could be established by performing cyclic analysis of deformed configurations at 100

and 200 cycles. Thus the original range of extrapolation was reduced and the thinout curve was adjusted by using calculated thinout rates at 100 and 200 cycles. The study also includes an analysis of the same undeformed chamber model constructed of half-hard Amzirc to study the effect of material properties on the thinout curve. Amzirc is a 0.15% zirconium copper alloy. The same loading cycle was applied to both the OFHC and Amzirc chambers. Additionally, a higher temperature cycle was applied to the Amzirc model.

3. PLUG NOZZLE THRUST CHAMBER

The structure analyzed during this study is the cylinder of a plug type thrust chamber shown in Fig. 1. The plug nozzle assembly consisting of the contoured centerbody and flanged cylinder is shown along with cross-sectional details of the cylinder. The contoured centerbody provides a variable cross section area along the length of the cylinder similar to that which exists in a conventional contoured thrust chamber in the throat region.

The basic component of the cylinder is the inner wall which contains 72 axial flow coolant channels of constant cross section. Two cylinders were analyzed during the study. One cylinder inner wall was constructed from fully annealed OFHC copper. The inner wall of the second cylinder was of half-hard Amzirc. The closeout wall of both cylinders was electroformed copper (EFCU).

3.1 THRUST CHAMBER MATERIAL PROPERTIES

The properties used to characterize the cylinder wall materials were provided by LeRC. The data, taken from Ref. 2, define typical temperature dependent thermal expansion, modulus of elasticity and static stress-strain behavior of annealed OFHC, half-hard Amzirc and as-formed EFCU. The material properties are presented in Figs. 2 through 10.

3.2 THERMOMECHANICAL LOADING CYCLES

The loading applied to the cylinder model consisted of constant amplitude thermomechanical cycles. A baseline cyclic load applied in 24 increments of temperature and pressure was supplied by LeRC. The baseline cycle was applied to the OFHC and Amzirc models.

A second cycle, also applied to the Amzirc model, consisted of the same 24 incremental load steps plus two additional increments at the end of the heating phase of the cycle. The two additional increments were added to account for an increase in maximum hot gas surface temperature from 805 K (1450 R) in the baseline cycle to 950 K (1710 R).

The loading was assumed axisymmetric and structural symmetry was exploited in order to treat the smallest representative segment of the chamber. The operating pressures defined in Fig. 11 were applied to the hot gas surface and coolant channel and were assumed to vary linearly with time during transition periods between cooling and heating phases. The duration of each transition period as well as the durations of cooling and heating phases were specified and are defined in Fig. 11.

Baseline two-dimensional temperature histories at selected throat plane nodes are shown in Fig. 12. The origin of the time scale, i.e., time = 0 on this plot is the beginning of the hot phase shown on the diagram accompanying Fig. 11.

4. STRUCTURAL ANALYSIS

A quasi three-dimensional structural analysis of the OFHC and Amzirc chambers was performed with the BOPACE finite element computer program. Generalized plane-strain isoparametric elements were used to model the smallest repeating segment of the cylinder wall, and time-varying nodal temperatures, elemental pressure loading and axial thermal strains were applied to compute chamber wall deformation histories under repetitive firing cycles. In addition, nonlinear variations in the temperature dependent material properties and mechanically and thermally induced plasticity were accounted for in the computations.

An initial chilldown from an assumed fabrication temperature of 294 K (530 R) to a uniform 28 K (50 R) with appropriate coolant surface pressure was applied to simulate initial starting conditions in the test thrust chambers. The entire chamber model remained elastic during the initial chilldown.

Ten identical firing cycles were then imposed on the OFHC and Amzirc models which were geometrically the same prior to initial chilldown. Three-dimensional behavior of the chambers was approximated by specifying a time varying axial strain equal to the average thermal strain of the relatively massive EFCU closeout wall. The BOPACE solution involved load incrementation, periodic updating of the stiffness matrix and residual load iteration to ensure equilibrium.

The cumulative defomations at the end of a firing cycle were used as the referent configuration for the succeeding cycle. The entire structure was at 28 K (50 R) with a coolant channel pressure of 5.10 MN/m^2 (740 psia) at the end of each cycle. The computed volume of the 10th cycle configurations

was used to check extrapolated configurations to assure that total mass was conserved during the analysis.

A schematic of the chamber model is shown in Fig. 13. Node and element numbers are identified. The inner wall region is comprised mainly of quadratic elements. Higher order elements were used on the hot-gas and coolant boundaries in an attempt to more accurately determine nodal displacements on these two surfaces. The closeout wall which exhibits no significant plastic deformation was modeled with linear elements. A computer plot of the undeformed model is presented in Fig. 14.

4.1 OFHC COPPER CHAMBER ANALYSIS

The first 10 firing cycles were consecutively applied to the model after the initial chilldown. Figs. 15, 16 and 17 show the computed radial displacements of the hot gas and coolant surfaces after initial chilldown and at the end of cycles 5 and 10. The progressive inward bulging of the channel wall and thinout of the wall at the channel centerline is apparent. Figure 18 shows the decreasing thickness of the chamber wall at the channel centerline during the first 10 cycles. The thinout rate of -2.7×10^{-3} mm/cycle (-1.05×10^{-4} in./cycle) is uniform over the first five cycles and then decreases to a value of -4.4×10^{-4} mm/cycle (-1.7×10^{-5} in./cycle) at the end of 10 cycles. The rate decrease was attributed to an increase in membrane loading of the chamber wall as the wall bulges under the firing cycles.

Nodal displacements of the chamber wall boundaries were used to define displacement rates of these boundaries at the end of the 10th cycle. The displacement rates were linearly extrapolated to 100 cycles and the model was redefined for this configuration. Figure 19 shows the predicted shape of the chamber wall for the 100-cycle configuration. The progressive plastic flow in the wall is demonstrated by the thinout of the model at the channel and rib centerlines. Figure 20 shows the predicted thickness distribution of the chamber wall after extrapolation to 100 cycles. The 100-cycle

model, shown in Fig. 21 had a cross sectional area of 1.0417×10^{-5} m^2 (0.016147 sq in.) which compared to the cross section area of 1.0422×10^{-5} m^2 (0.016155 sq in.) at the end of 10 cycles. This difference, 0.048 percent, indicates that mass was reasonably conserved in the extrapolation.

The 100-cycle model was subjected to five consecutive firing cycles to determine displacement rates of the deformed chamber walls. The computed thinout rate changed from -4.4×10^{-4} mm/cycle (-1.7×10^{-5} in/cycle) at the 10th cycle to -1.2×10^{-3} mm/cycle (-4.9×10^{-5} in./cycle) at the end of 105th cycle. These computed rates were then used to interpolate between the 10th and 100th cycle configuration. The thickness interpolation function from 10 to 100 cycles was derived by assuming the function to be smooth and expressible as a quadratic within the range of interpolation. The time derivative of the assumed function results in a boundary value problem solved by using computed results for the 10th cycle thickness and the rate of change in thickness at 10 and 100 cycles. The resulting function of chamber wall centerline thickness is

$$t_1 = (-1.76 \times 10^{-7})\, n_1^2 - (1.37 \times 10^{-5}) n_1 + 0.0342$$

where

t_1 = thickness from 10 to 100 cycles (in.)
n_1 = cycle number, $10 \leq n_1 \leq 100$

The linear extrapolation procedure was then applied to the 100-cycle configuration and the 200-cycle configuration was developed. Figures 22 and 23 show the predicted shape and thickness distribution of the 200-cycle chamber wall. The 200-cycle model, shown in Fig. 24 had a total area of 1.0477×10^{-5} m^2 (0.01624 sq in.).

Five firing cycles were applied to the 200-cycle configuration to define the thinout rate at the channel centerline. The computer thinout rate at the end of the 205th cycle was -6.1×10^{-4} mm/cycle (-2.4×10^{-5} in./cycle). Interpolation of the 105th and 205th cycle analytical data resulted in a centerline thickness function of

$$t_2 = (1.27 \times 10^{-2}) n_2^2 - (7.44 \times 10^{-5}) n_2 + .0372$$

where

t_2 = thickness from 100 to 200 cycles (in.)

n_2 = cycle number, $100 \leq n_2 \leq 200$

Functions t_1 and t_2 are shown plotted in Fig. 25. The thickness from cycle 0 to 10 was obtained from computed data in this range.

The complex elements used to model the chamber provided satisfactory nodal displacement data, but interpretation of the stress field was difficult. The problem of interpreting stresses was alleviated by developing a finer mesh 200-cycle model with linear quadrilateral elements. The goal was to determine the maximum stresses, critical locations, and the time of occurence during a single cycle load application to the 200-cycle configuration. The linear-element model is shown in Fig. 26. A plot of the histories of circumferential stresses at the channel centerline on the hot gas and coolant surfaces is shown in Fig. 27. It is seen that maximum tensile stresses of 5.52 Pa (8 ksi) occur approximately 0.2 seconds after the end of the heating phase. The calculated temperature of the channel wall is 238 K (430 R) at the critical time. According to Ref. 2, the uniaxial tensile strength of OFHC at this temperature is 2.4×10^8 Pa (35 ksi) and rupture of the wall would not be expected. If, however, low-cycle fatigue damage results in the development of a crack at the 200-cycle range, flaw growth would probably be quite rapid and give the appearance of a strength failure in the channel wall. It was observed that an average calculated effective strain range of 1.6% was essentially the same for models used in the analyses of cycles 1 through 10 and cycles 201 through 205. A previous analysis (Ref. 3) shows that the formation of a fatigue crack

under the applied loading should occur at approximately 200 cycles. Thus it is possible that an OFHC channel wall would crack through in the thinned region at about 200 cycles. The failure mechanism would be complex and the stages would probably consist of concurrent thinning and low-cycle fatigue damage which produce a flaw with rapid growth rates in the thinned out region.

4.2 HALF-HARD AMZIRC CHAMBER ANALYSIS

The Amzirc chamber was analyzed for two different firing conditions. The pressures and temperatures were the same as those used for the OFHC chamber for one condition. The second firing condition was the same except that the coolant wall temperatures were modified to account for an increase in the hot gas surface temperature from 805 K (1450 R) to 950 K (1710 R). The two different firing conditions were defined as baseline and high temperature firing cycles.

Ten baseline cycles of loading applied to the Amzirc model resulted in much smaller plastic deformation than calculated for the OFHC model. Figure 28 is a plot of chamber wall thickness at the channel centerline. The computed Amzirc thickness reduction at the end of 10 cycles is only 7.14 percent of the corresponding value computed for the OFHC model. This difference in behavior was attributed to the greater stiffness and higher yield strength of the Amzirc. Figures 29, 30 and 31 show the computed radial displacements of the hot gas and coolant surfaces at the end of initial chilldown and baseline cycles 5 and 10. The bulging and plastic flow are apparent but significantly smaller than observed in the OFHC chamber.

The baseline cycle deformations were linearly extrapolated to define the 100-cycle Amzirc configuration. Five successive baseline load cycles were applied to the 100-cycle model. The computed thinout rate at the channel centerline changed from -2.7×10^{-4} mm/cycle (-1.05×10^{-5} in/cycle) to zero at the end of the 105th baseline cycle. Thus plastic flow apparently ceased within the first 100 baseline firing cycles of the Amzirc chamber.

The above data were used to develop an interpolation function for centerline thinout of the Amzirc channel wall. The derived function from cycle 10 to 100 is

$$t = (5.85 \times 10^{-8})n^2 - (1.17 \times 10^{-5})n + 0.03491$$

The centerline wall thickness is shown in Fig. 32.

The high temperature load cycle was applied to the Amzirc model after initial chilldown to 28 K (50 R) and 10 successive firings were applied. Figures 33 and 34 show radial displacements at the end of cycles 5 and 10. Figure 35 compares the decrease in thickness of the wall at the channel centerline for the model subjected to both temperature cycles.

The deformation rates at the end of the 10th high-temperature cycle were extrapolated to define the 100-cycle configuration shown in Fig. 36. Ten successive high-temperature loading cycles applied to the extrapolated model resulted in a computed thinout rate of -4.8×10^{-4} mm/cycle (-1.9×10^{-5} in./cycle) and the thinout rate at the end of the first 10 cycles was -5.6×10^{-4} mm/cycle (-2.2×10^{-5} in./cycle). The thickness function for the range of 10 to 100 high temperature cycles is

$$t = (1.72 \times 10^{-8})\, n^2 - (2.27 \times 10^{-5})\, n + 0.03499$$

The curve of wall centerline thickness is shown in Fig. 37.

5. CONCLUDING REMARKS

The results of the present study and the work reported in Ref. 1 demonstrated the ability to predict cumulative plastic deformations of cyclically loaded structures. The BOPACE program, which provides state-of-the-art technology in finite element nonlinear analysis, enabled the progressive bulging and plastic flow to be determined for successive firings of the engine thrust chamber.

The nonlinear isoparametric elements used to model and compute engine chamber deformations provided results that are believed to be good predictions of long-term engine response to the specified load cycle. These elements enable the modeling of structures of complex shapes and large gradients with relatively coarse mesh sizes. This modeling advantage is offset, however, by difficulty in interpreting the stresses and strains in the structure. Since the elements can be relatively large, the deformation gradients within a given element can be large and the state within the element can range from elastic to plastic conditions. Thus large jumps in computed stresses usually exist across element boundaries. In order to alleviate the stress analysis problem, it was necessary to use the deformed boundaries and develop a fine mesh linear element model. The computed results indicated that the maximum hoop stress is not sufficient to cause strength rupture of the OFHC chamber wall after predicted thinout resulting from 200 firings. The analysis indicates that failure is precipitated by formation of a low-cycle fatigue crack which rapidly grows through the wall. It is recommended that several OFHC chambers be tested and each bisected at a predetermined number of cycles so that the progressive thinning and bulging may be observed prior to 200 cycles for comparison to the predicted conditions.

The Amzirc model analysis indicates that the higher strength inner wall exhiblts significant reductions in bulging and thinout. Behavior of the Amzirc chamber was sensitive to the magnitude of the hot gas surface temperatures and temperature gradients, however. It is probable that both chambers would exhibit more permanent distortion if the structural temperatures were updated along with the structural model update. Although the channel distortion would have negligible effects on the boundary conditions, the wall temperature and temperature gradients will change with the geometric configuration. It is recommended that additional analyses be performed to define the importance of cyclic load updating.

It was noted that the effective strain range resulting from application of the specified cycle to the initial and deformed models of the OFHC chamber was essentially constant. It is possible to perform configuration trade studies which evaluate the susceptibility of a chamber design to permanent distortion and damage under constant or variable cycle loading. Structural configurations which are recommended for future study include the milled chamber wall with a curved (instead of rectangular) coolant wall; the addition of slots at the rib centerline to relieve the chamber wall; and a brazed coolant tube configuration. The present study provides the analytical capability to efficiently evaluate the long-term behavior of these configurations. The development of such information will add to the LeRC thrust chamber design and analysis methodology.

6. REFERENCES

1. Vos, R.G., and W.H. Armstrong, "Structural Analysis of an OFHC Copper Cylinder Thrust Chamber," Boeing Report D180-20708-1, Contract NAS3-20404, NASA-Lewis Research Center, Cleveland, Ohio, July 1977.

2. Esposito, J.J., and Zabora, R.F., "Thrust Chamber Life Prediction – Mechanical and Physical Properties of High Performance Rocket Nozzle Materials," NASA CR-134806, Contract NAS3-17838, NASA-Lewis Research Center, Cleveland, Ohio, March 1975.

3. Armstrong, W.H., and E.W. Brogren, "Three-Dimensional Thrust Chamber Life Prediction," Contract NAS3-19717, NASA-Lewis Research Center, Cleveland, Ohio, March 1976.

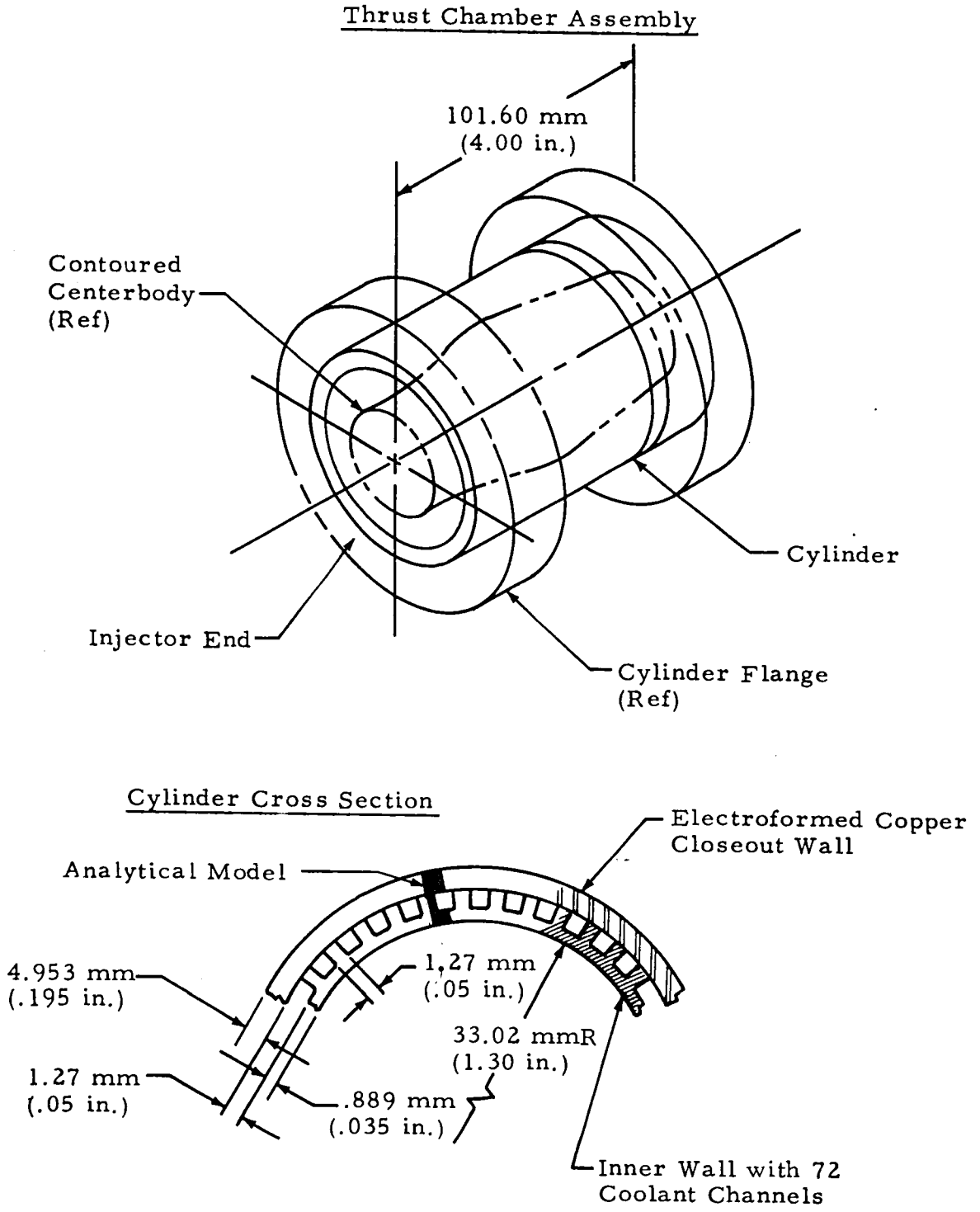

Fig. 1 - Plug Nozzle Thrust Chamber

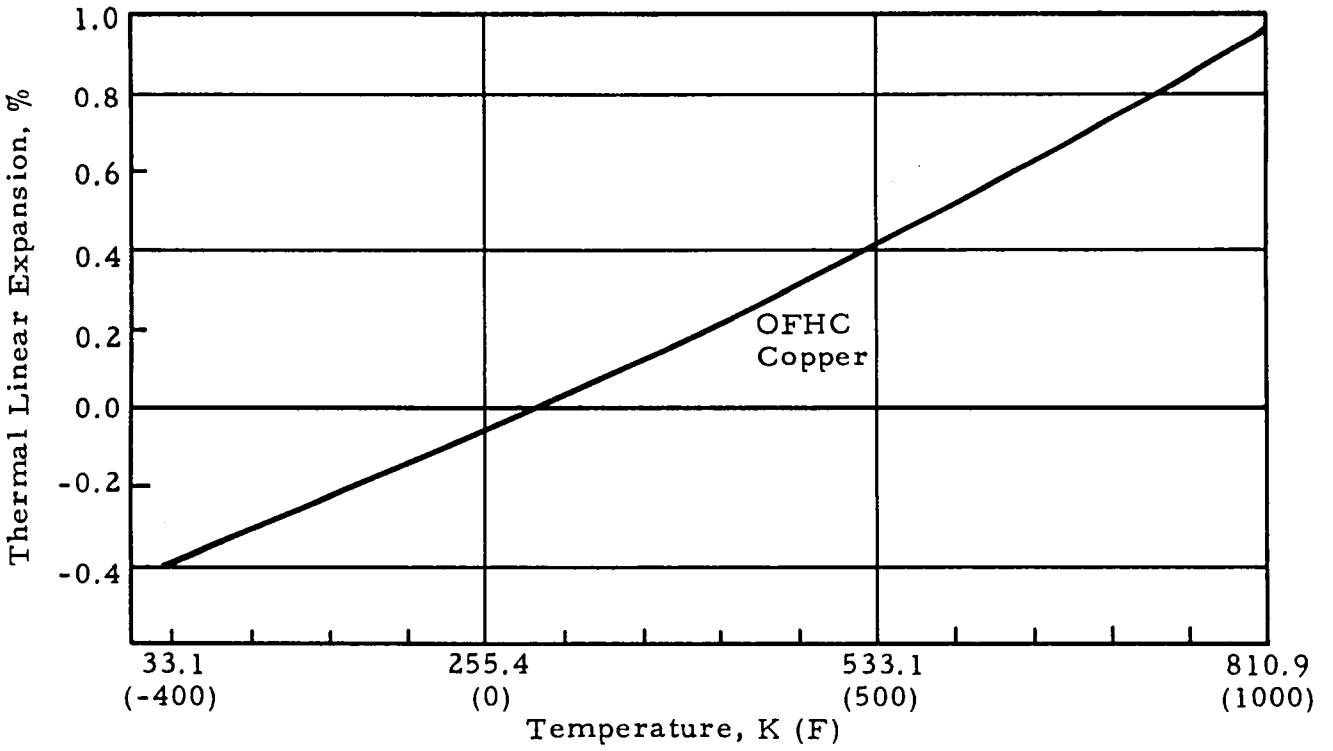

Fig. 2 - Thermal Linear Expansion vs Temperature for OFHC Copper

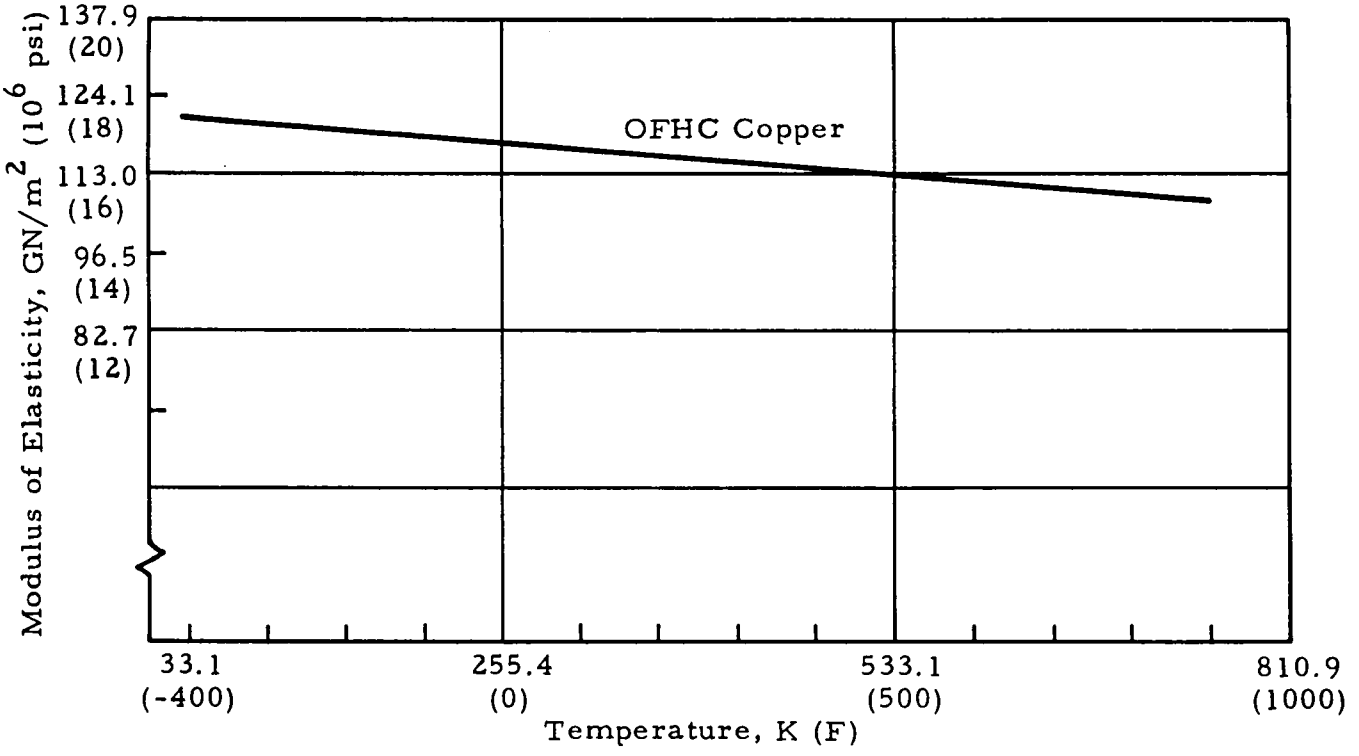

Fig. 3 - Modulus of Elasticity vs Temperature for OFHC Copper

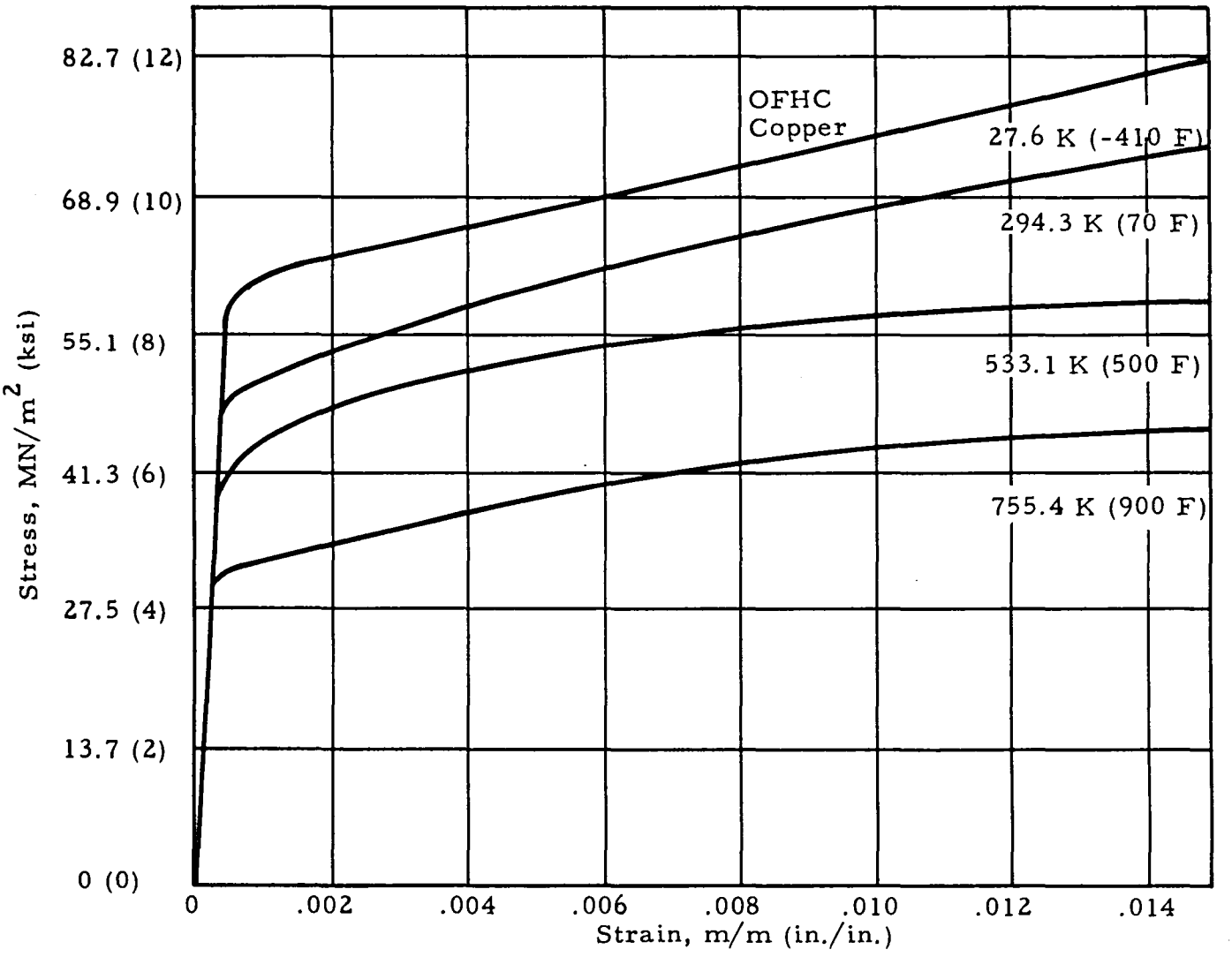

Fig. 4 - Typical Stress-Strain Cruves for OFHC Copper Annealed Condition

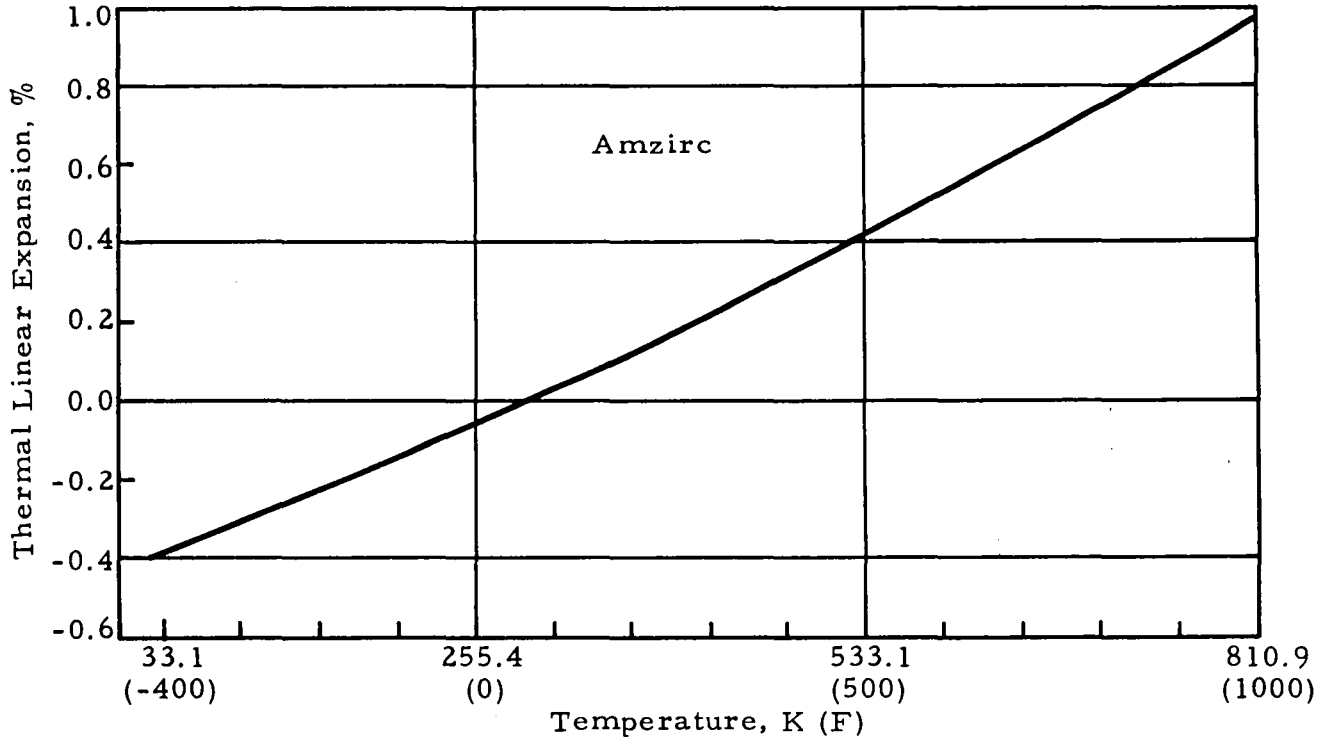

Fig. 5 - Thermal Linear Expansion vs Temperature for Amzirc

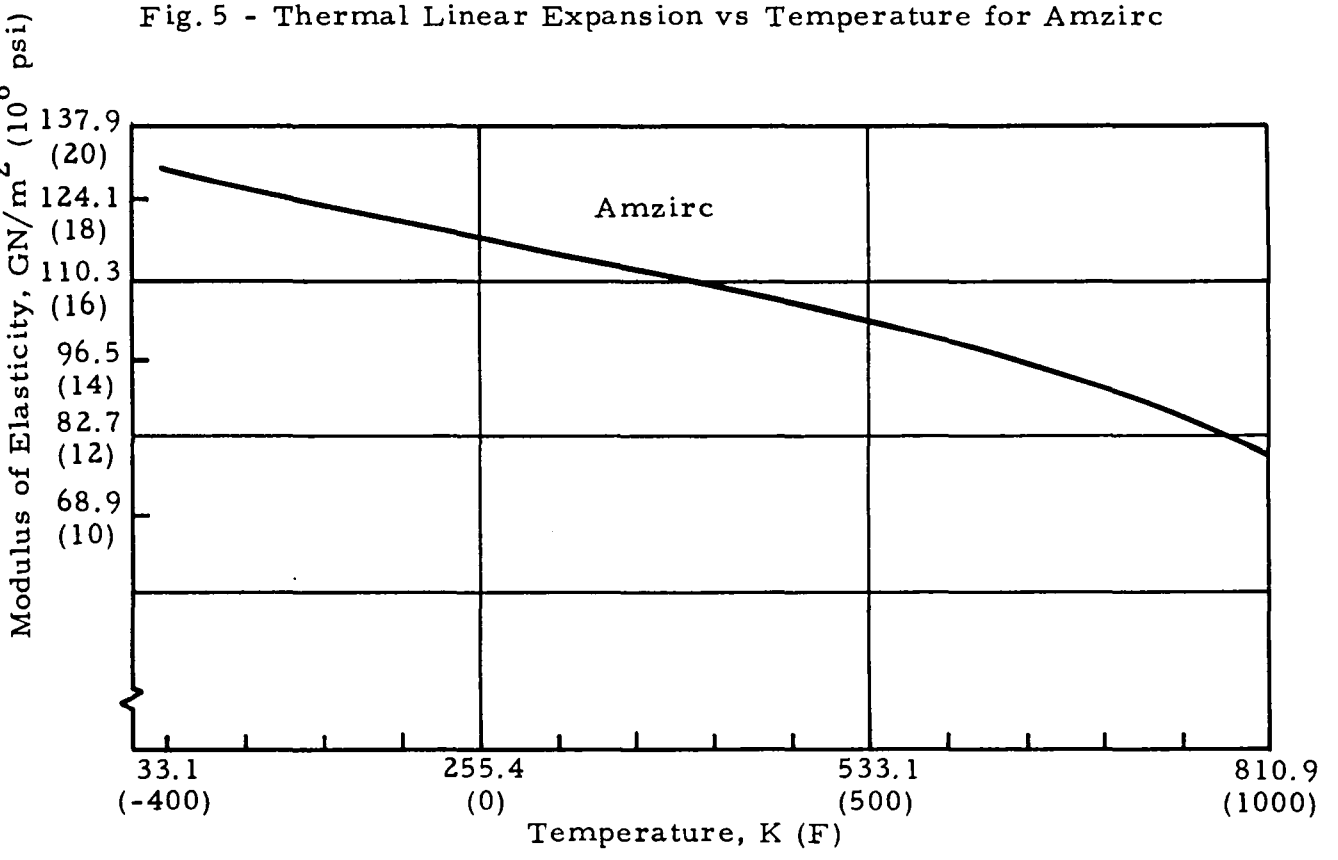

Fig. 6 - Modulus of Elasticity vs Temperature for Amzirc

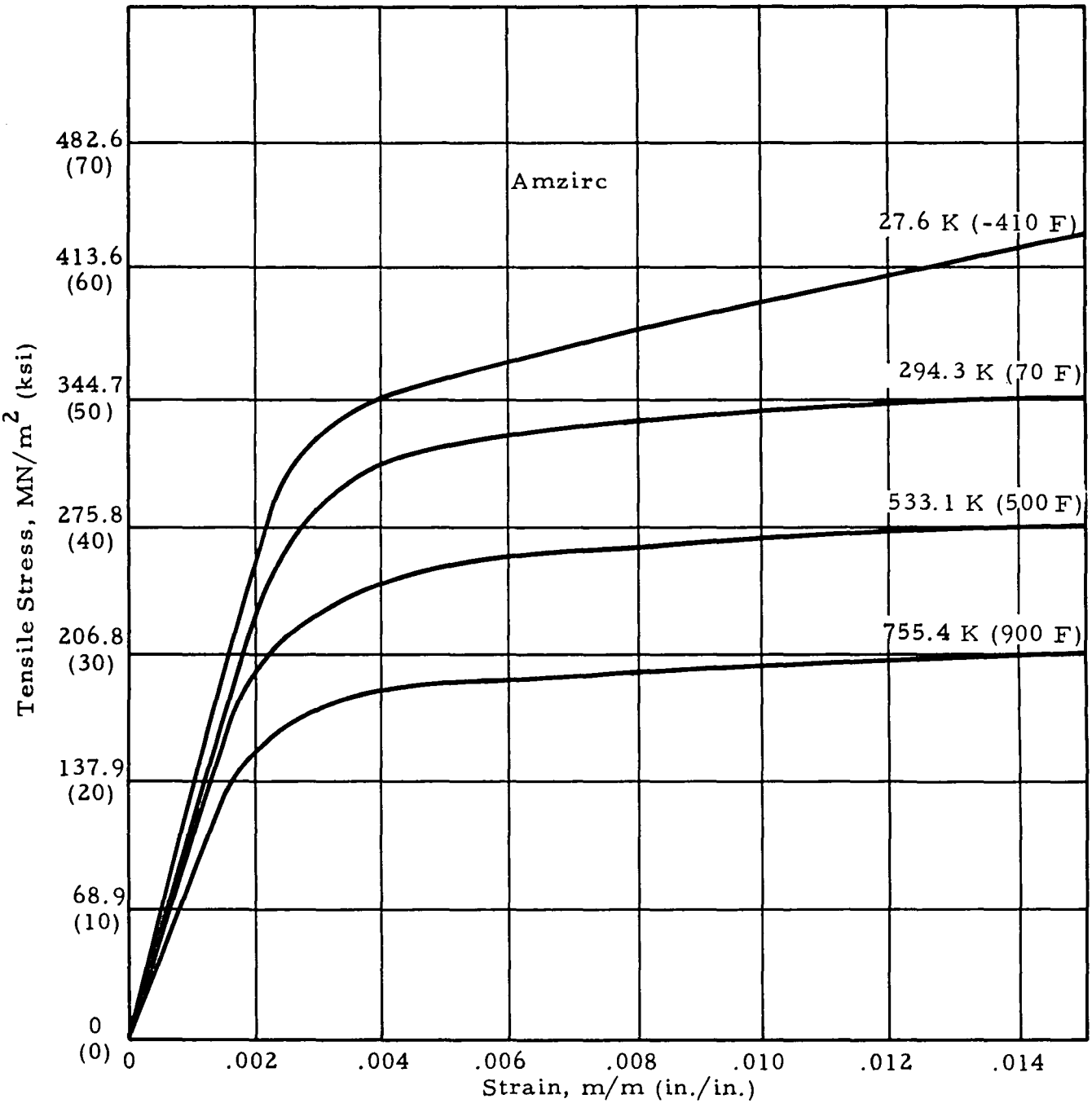

Fig. 7 - Typical Tensile Stress-Strain Curves for Amzirc-Half Hard Condition

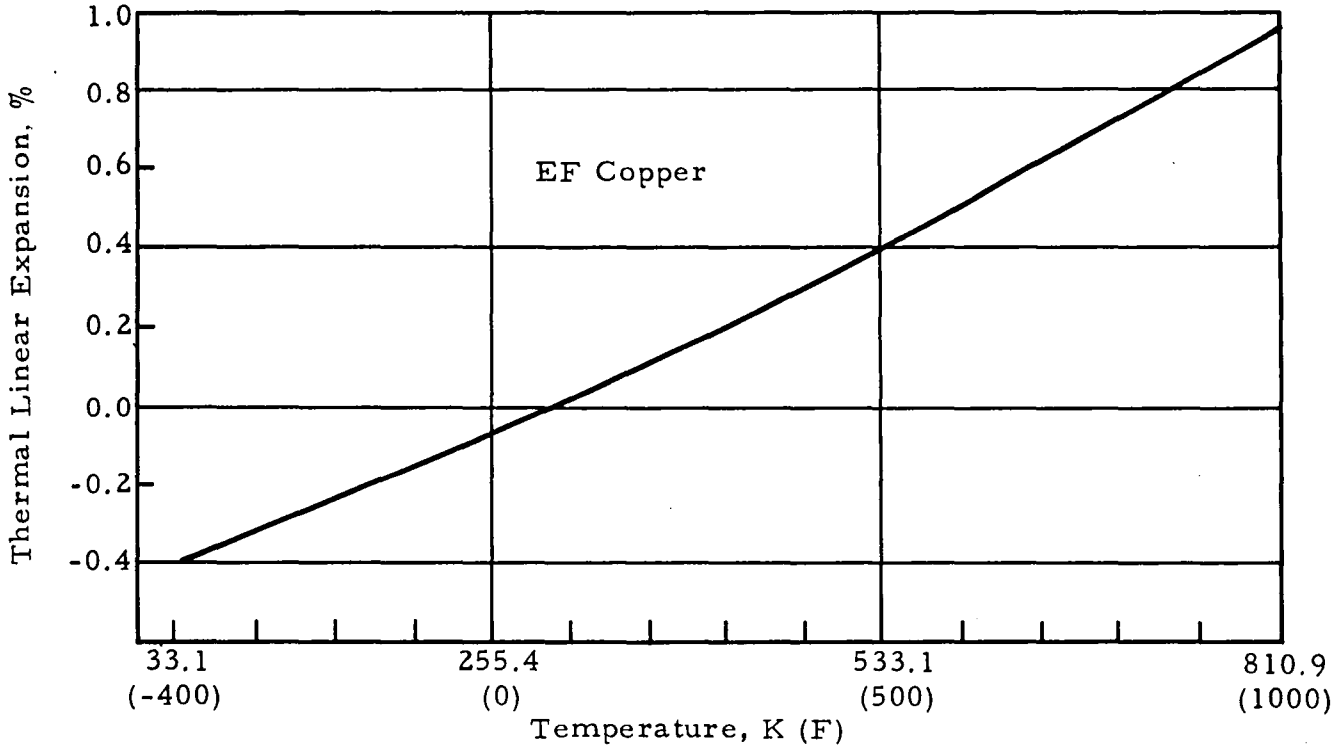

Fig. 8 - Thermal Linear Expansion vs Temperature for Electroformed Copper

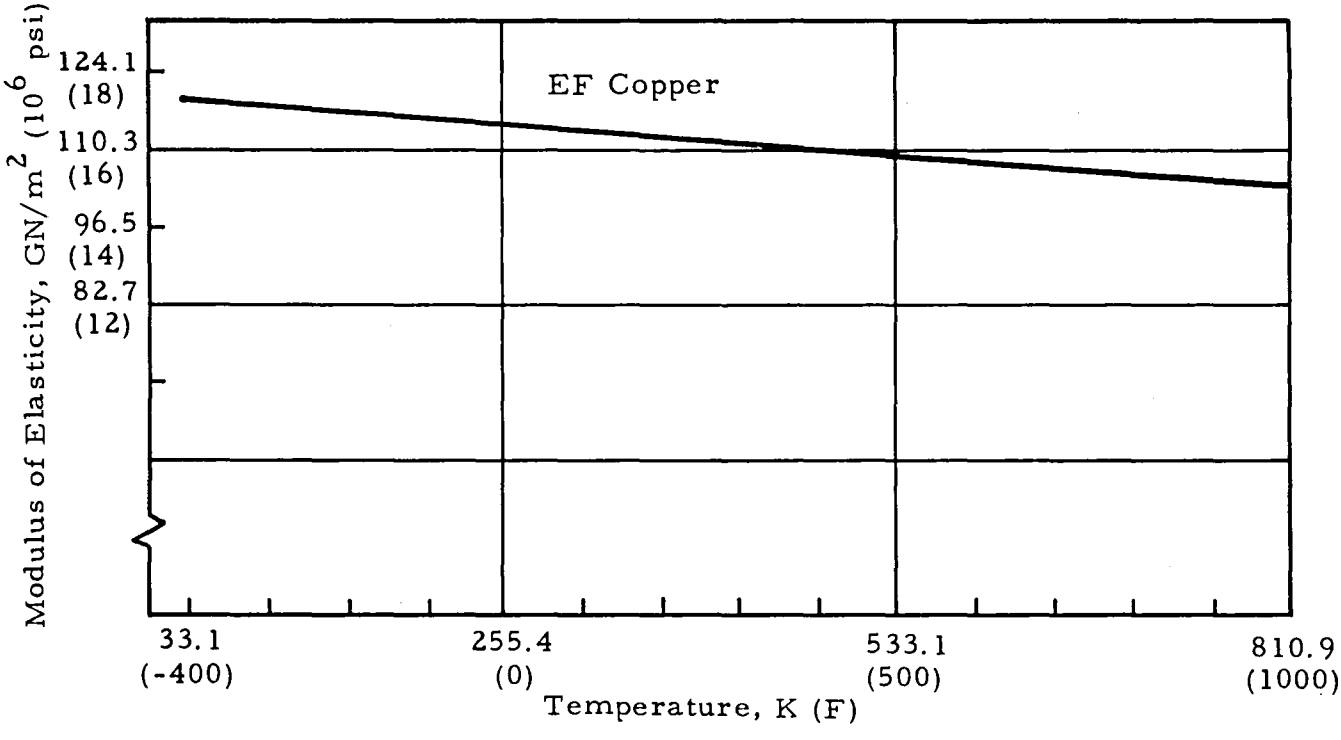

Fig. 9 - Modulus of Elasticity vs Temperature for Electroformed Copper

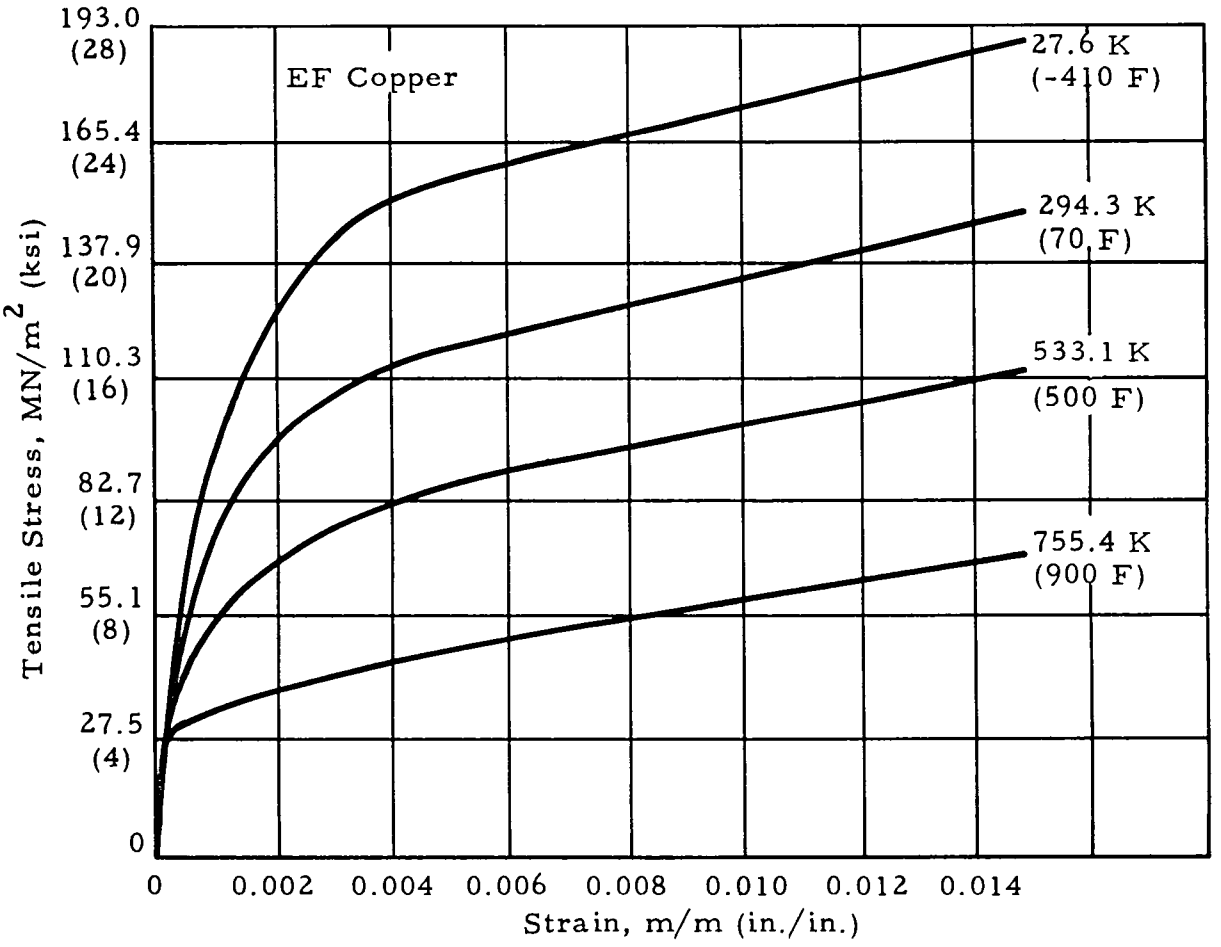

Fig. 10 - Typical Stress-Strain Curves for Electroformed Copper — as-Formed Condition

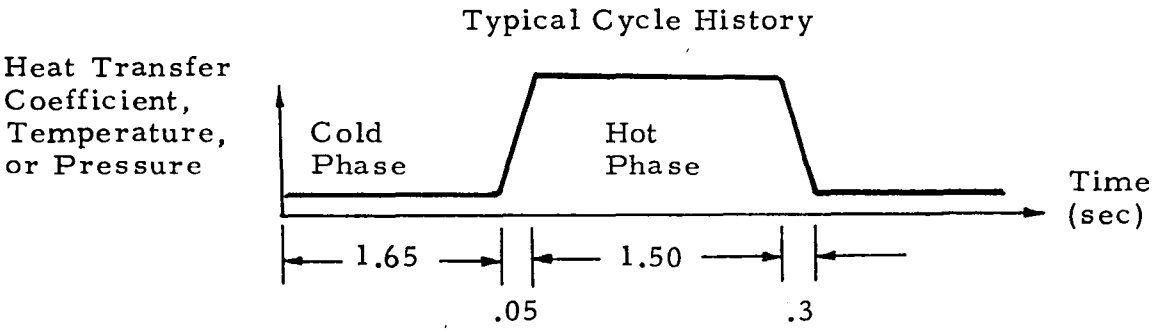

Cycle Phase	Cold	Hot
Hot Gas Side Heat Transfer Coefficient W/cm^2-K (Btu/in^2-sec-R)	0.0	2.02 (0.00685)
Hot Gas Side Adiabatic Wall Temperature K (R)	278 (500)	3364 (6055)
Hot Gas Side Wall Pressure kN/m^2 (psia)	96.5 (14.0)	2780 (403)
Coolant Side Heat Transfer Coefficient W/cm^2-K (Btu/in^2-sec-R)	10.2 (.0345)	4.83 (0.0164)
Coolant Side Bulk Temperature K (R)	28 (50)	50 (90)
Coolant Side Wall Pressure kN/m^2 (psia)	5100 (740)	6550 (950)

Fig. 11 - Boundary Conditions for Cyclic Structural Temperatures and Pressures

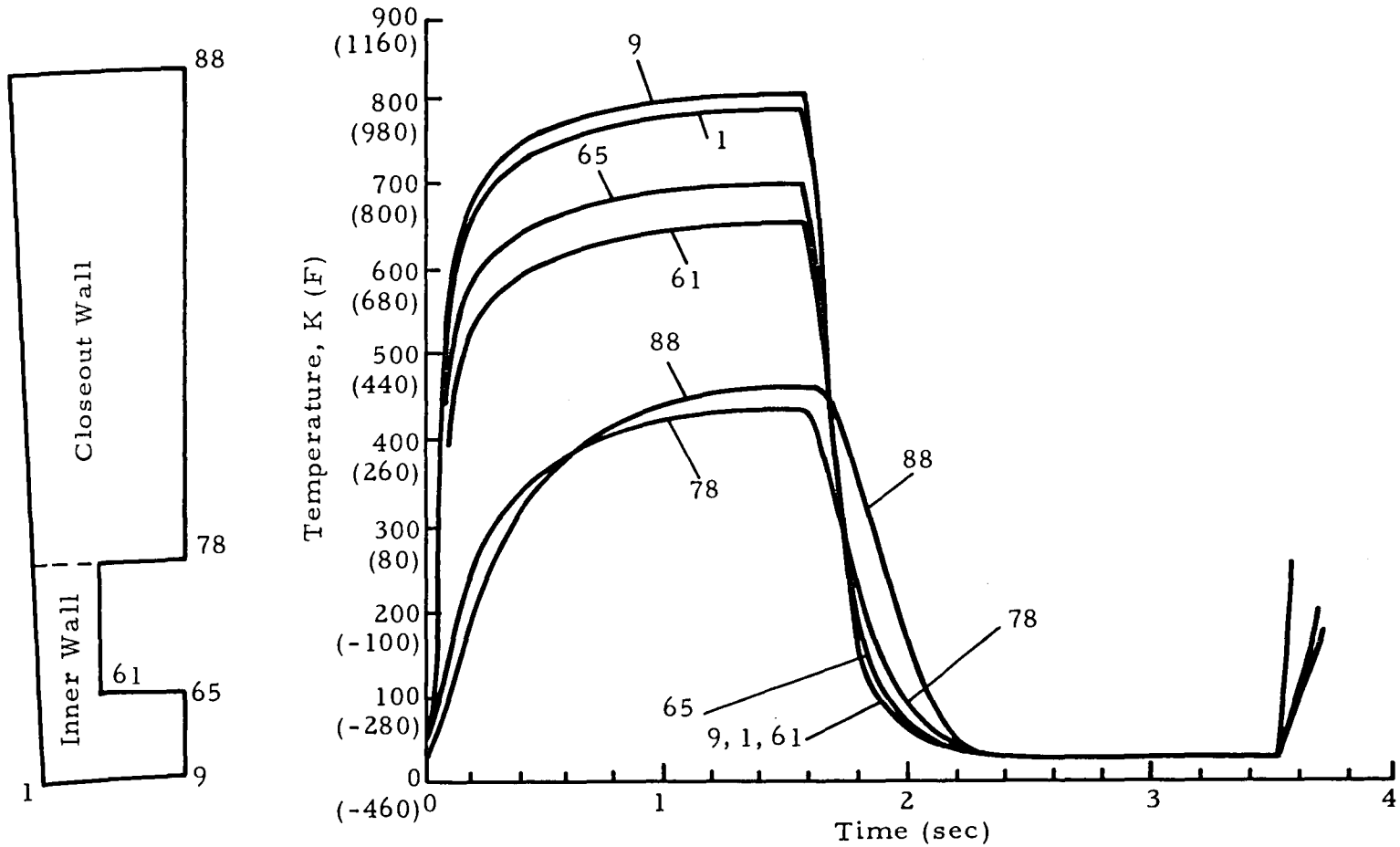

Fig. 12 - Typical Temperature Histories for Specified Boundary Conditions

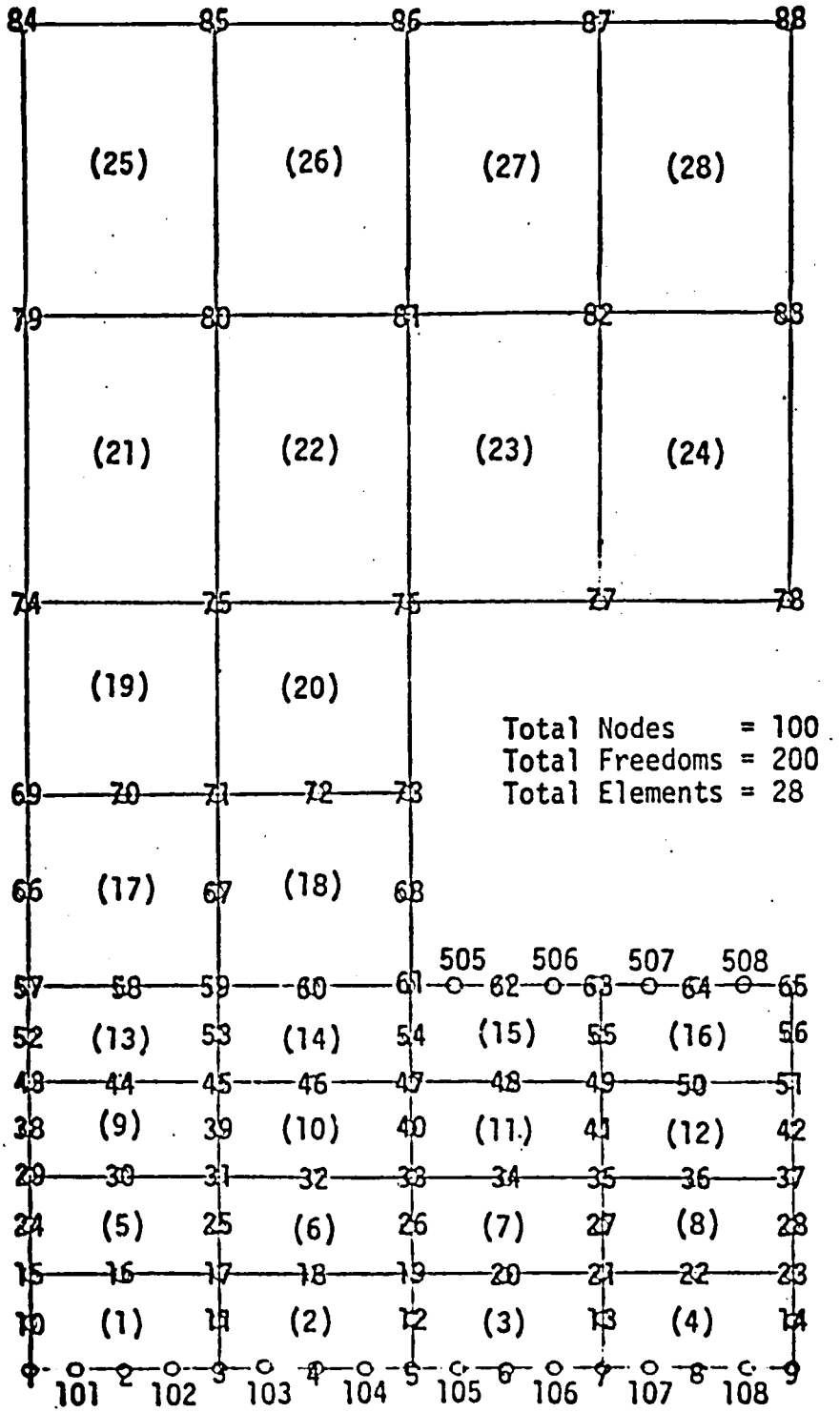

Fig. 13 - Schematic of BOPACE Model Showing Node and Element Identification Numbers

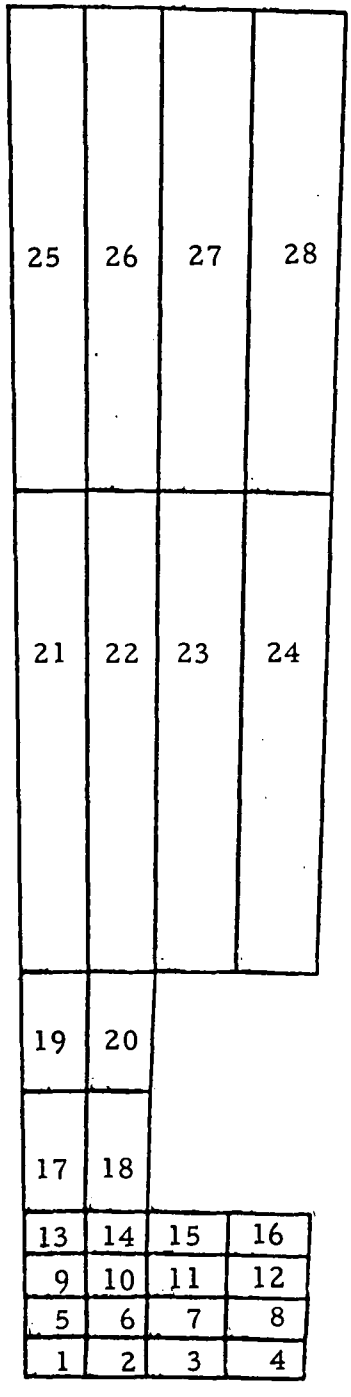

Total Nodes = 100

Total Freedoms = 200

Total Elements = 28

Fig. 14 - Computer Plot of Undeformed Thrust Chamber Model

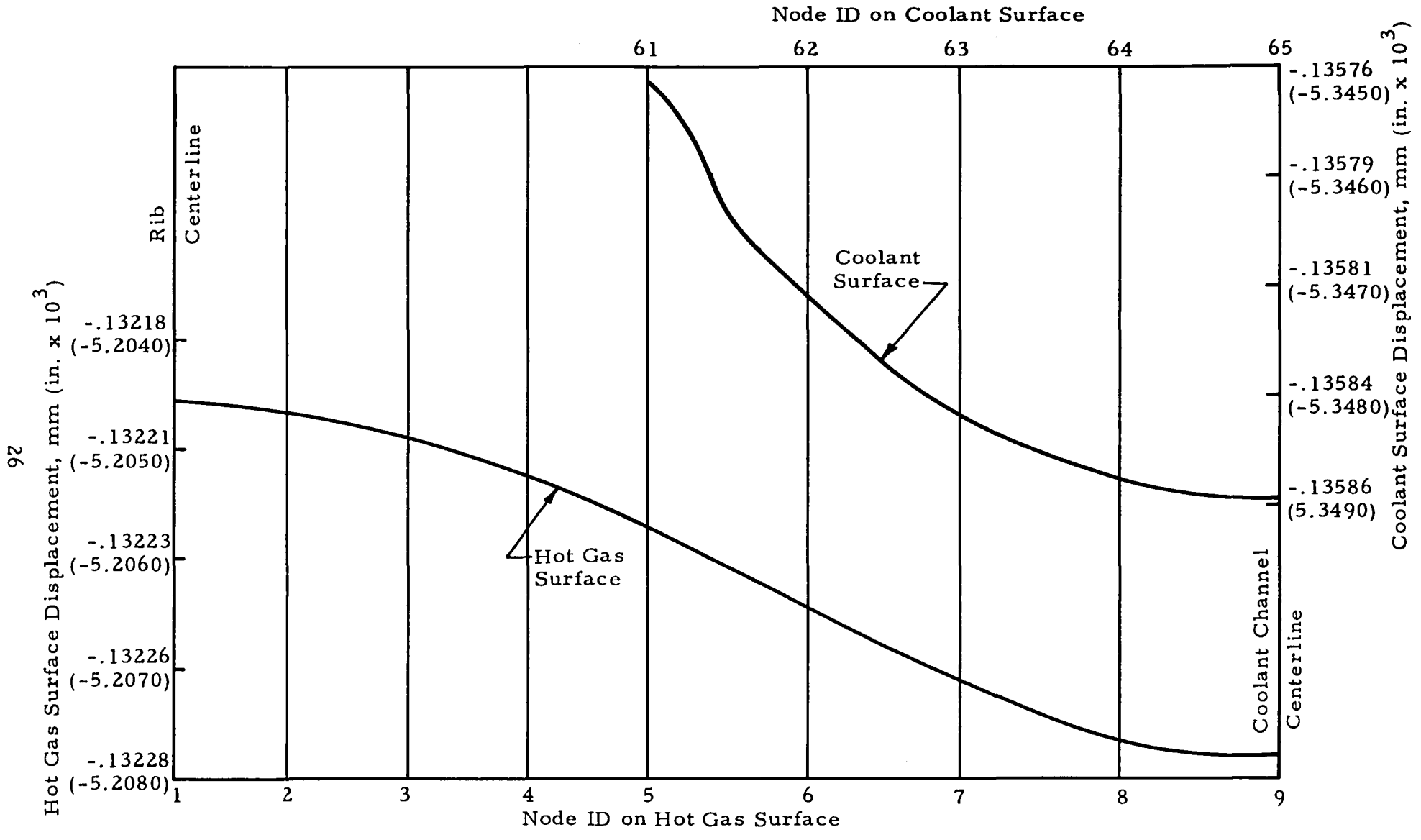

Fig. 15 - Radial Displacement of Hot Gas and Coolant Surfaces after Initial Chilldown to 28 K (OFHC Chamber)

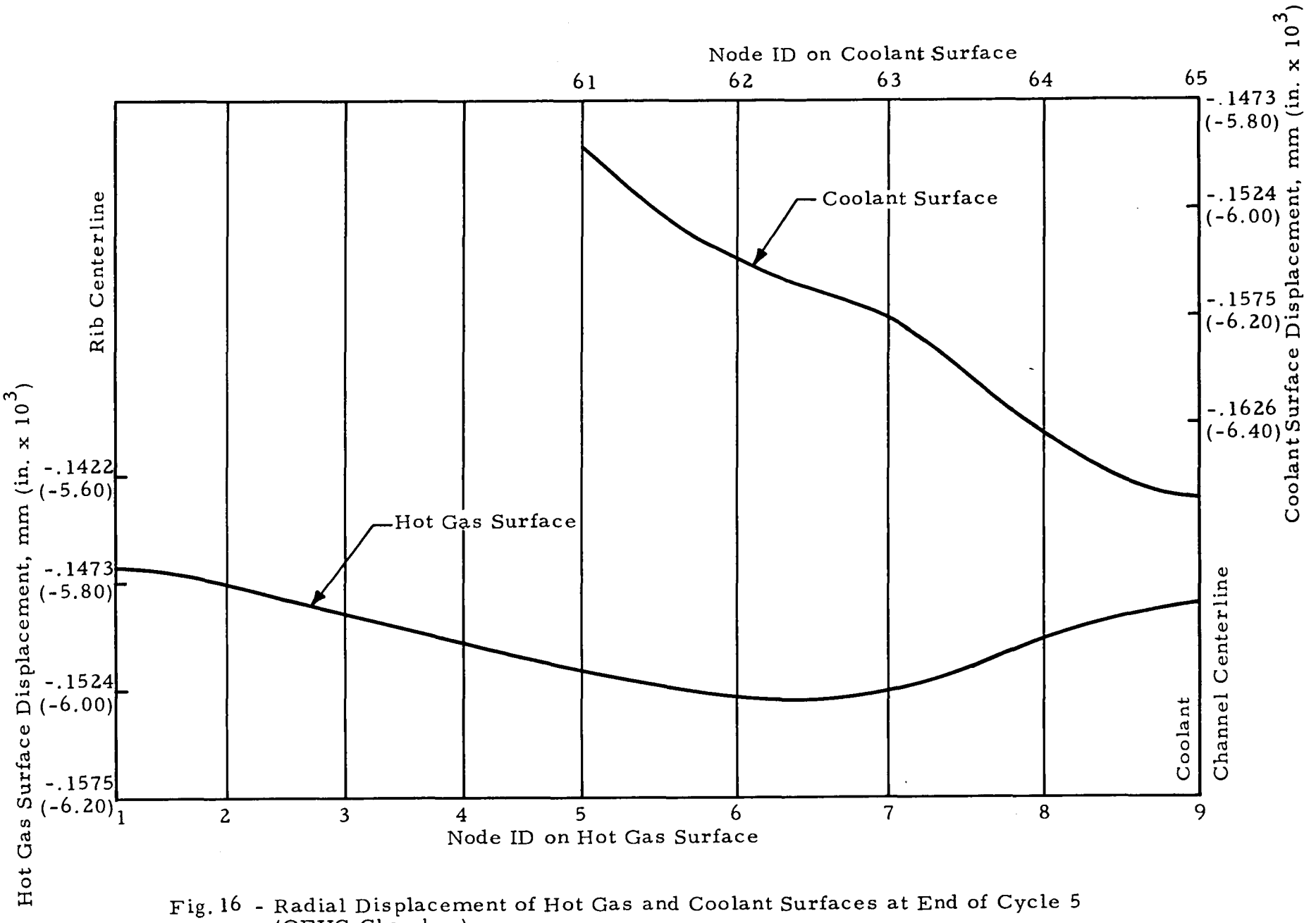

Fig. 16 - Radial Displacement of Hot Gas and Coolant Surfaces at End of Cycle 5 (OFHC Chamber)

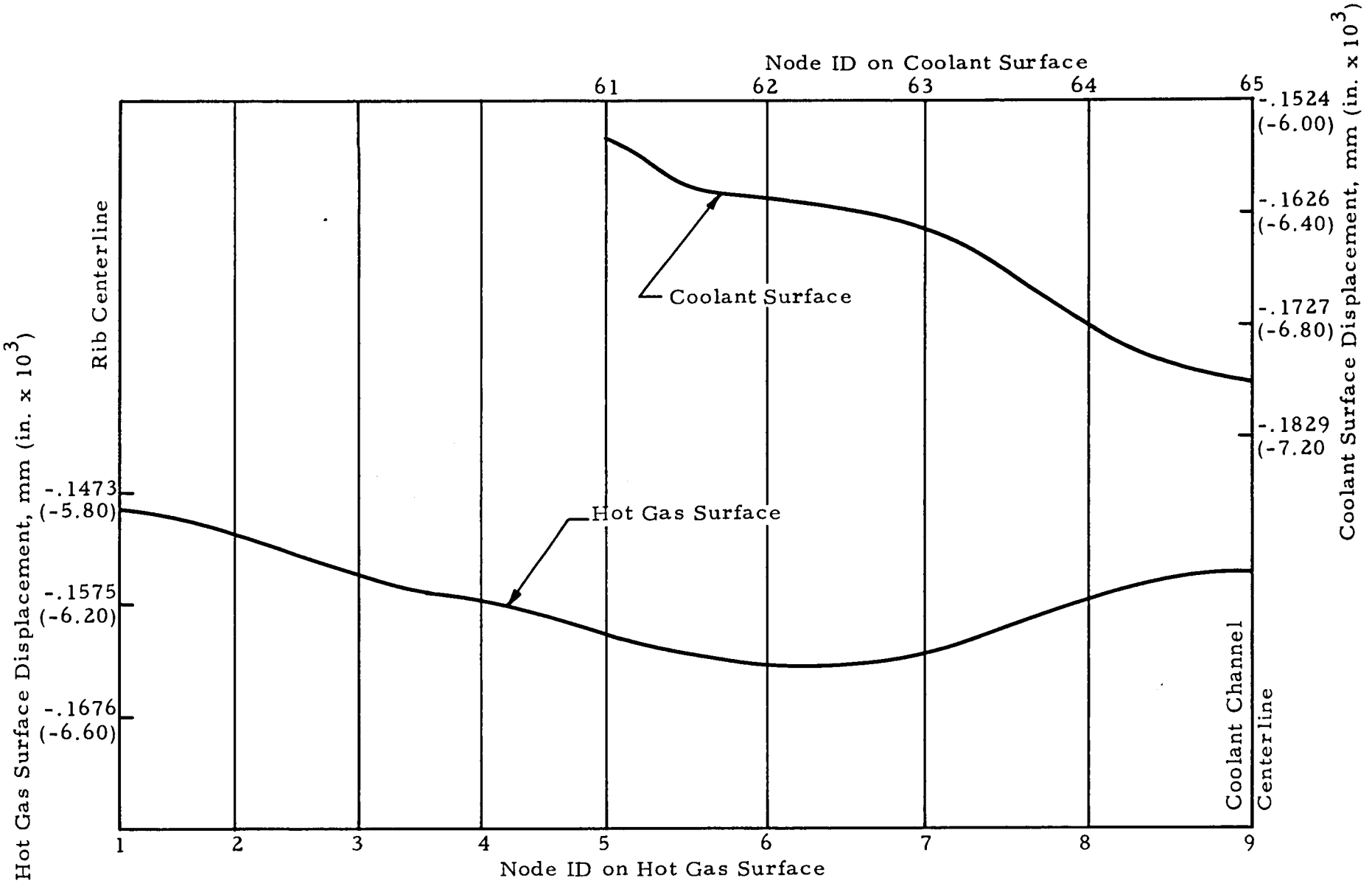

Fig. 17 - Radial Displacement of Hot Gas and Coolant Surfaces at End of Cycle 10 (OFHC Chamber)

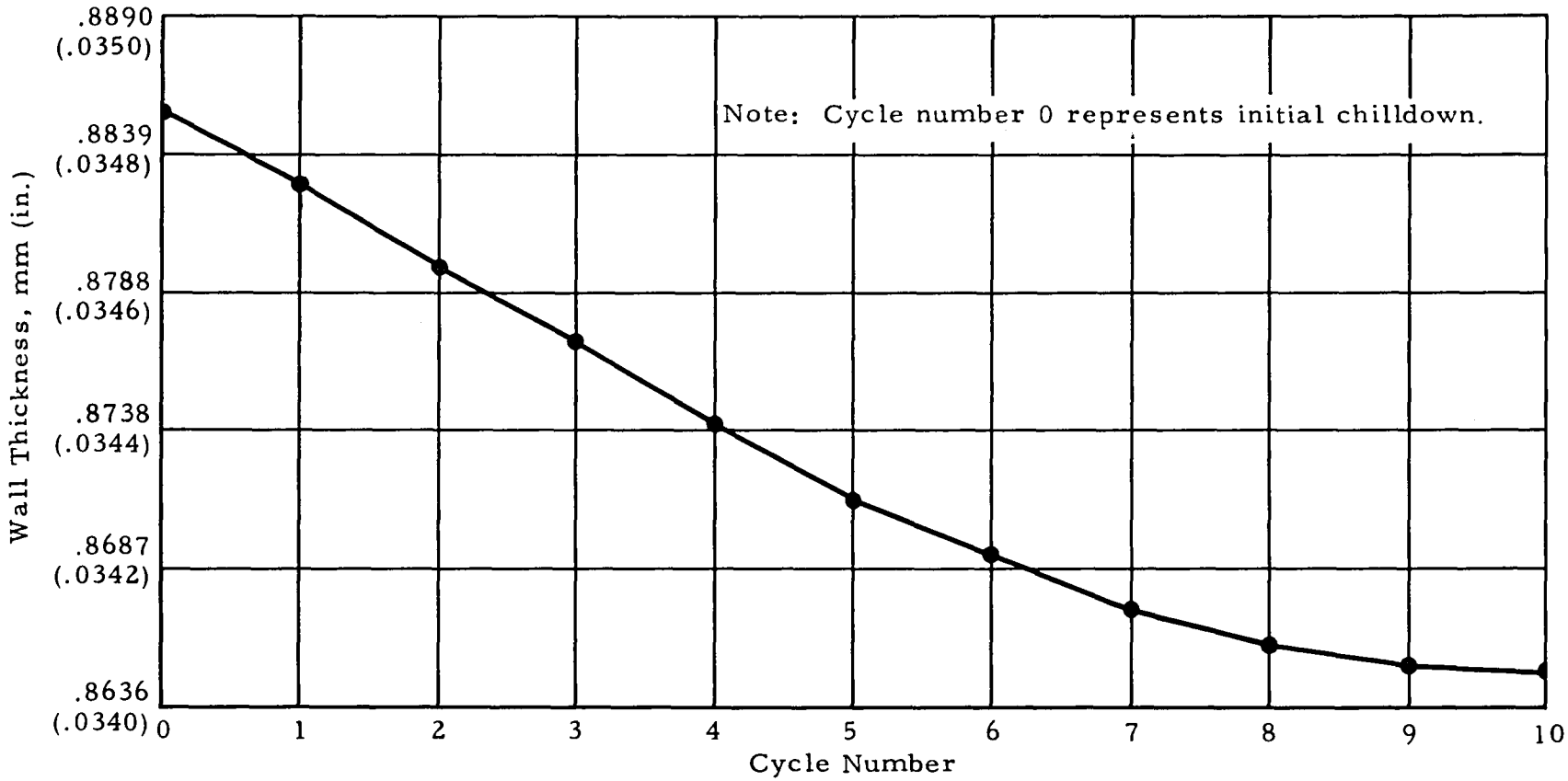

Fig. 18 - Computed Thickness of OFHC Inner Wall at Channel Centerline

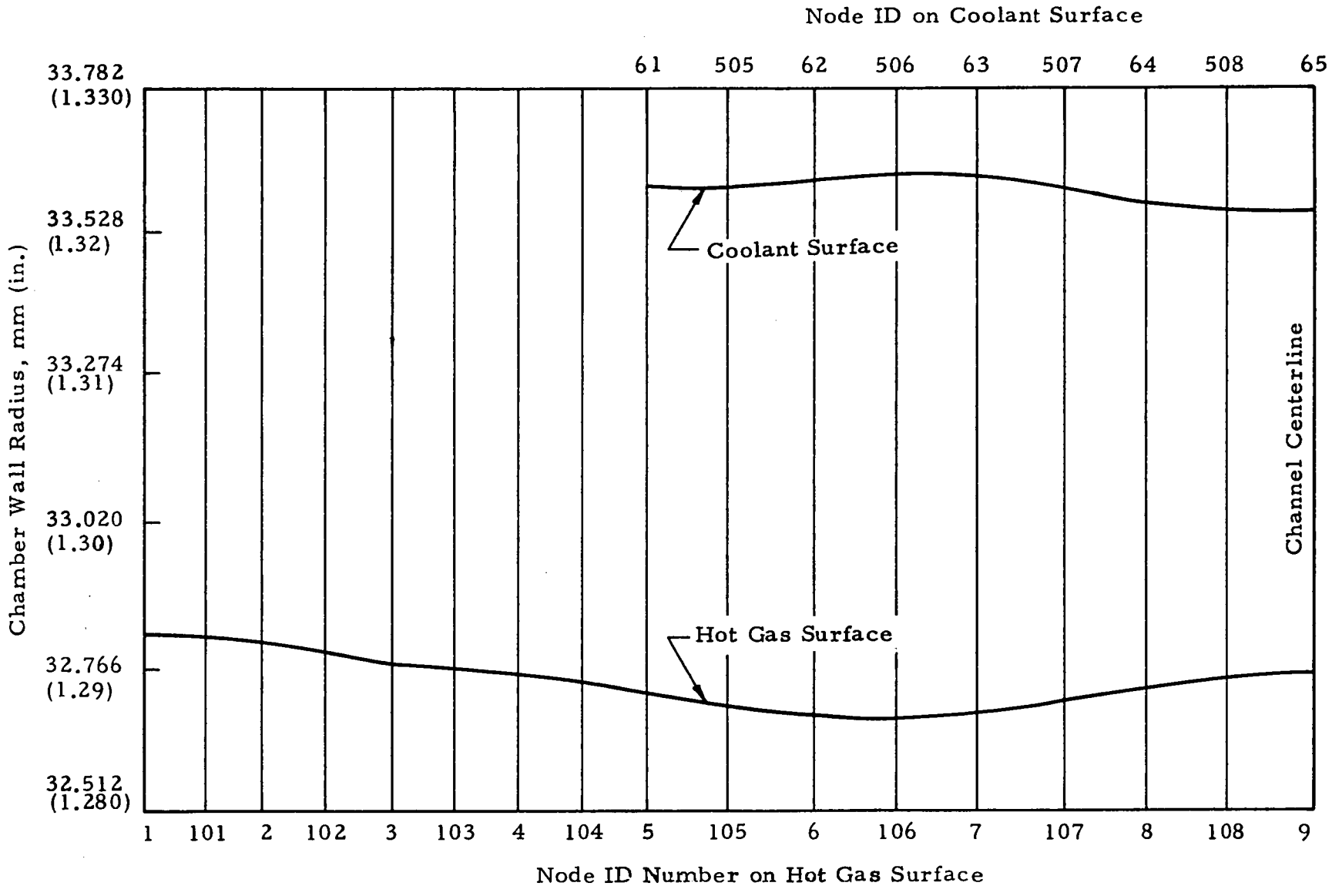

Fig. 19 - Predicted Shape of Inner Wall Region at the End of 100 Cycles on the OFHC Chamber

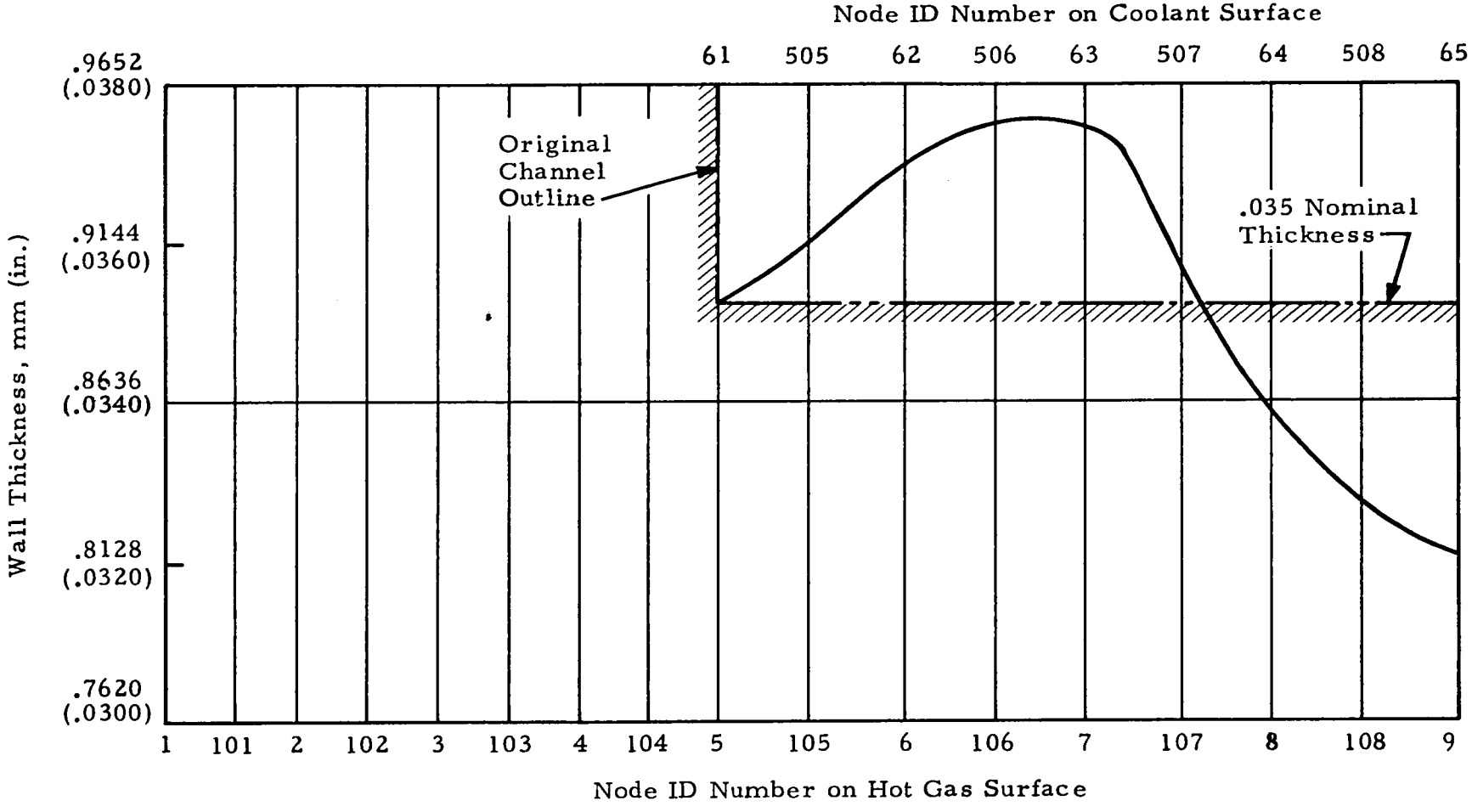

Fig. 20 - Predicted Thickness of Inner Wall Region at the End of 100 Cycles on the OFHC Chamber

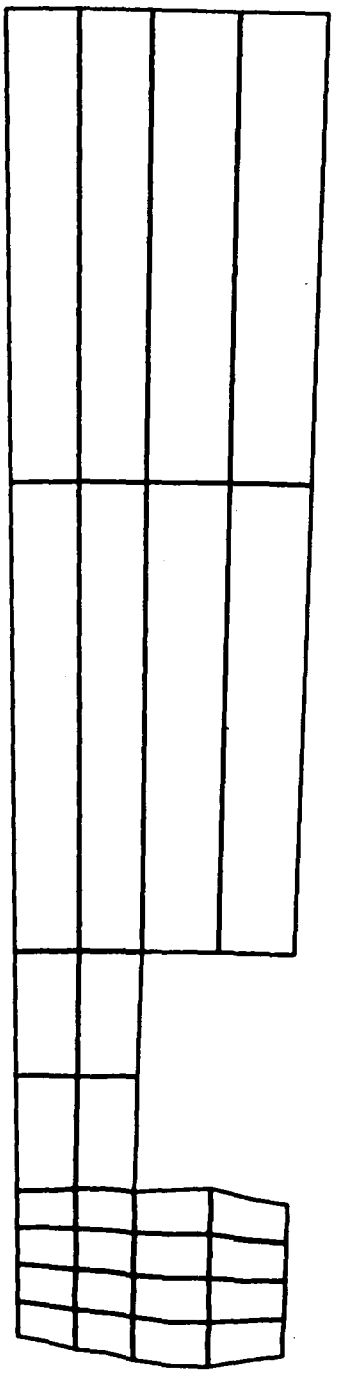

Fig. 21 - Computer Plot of 100-Cycle Configuration of OFHC Thrust Chamber

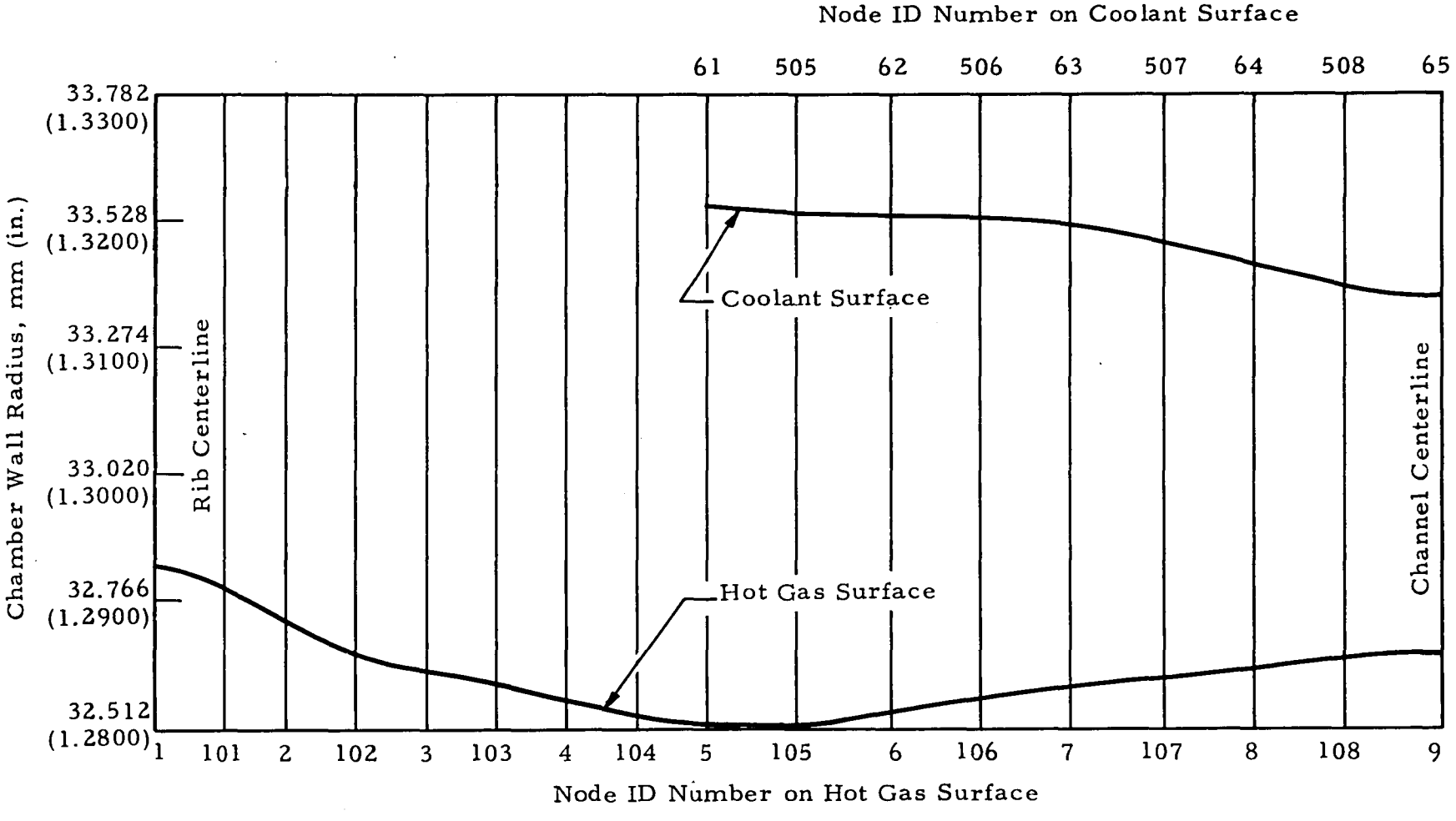

Fig. 22 - Predicted Shape of Inner Wall Region at the End of 200 Cycles on the OFHC Chamber

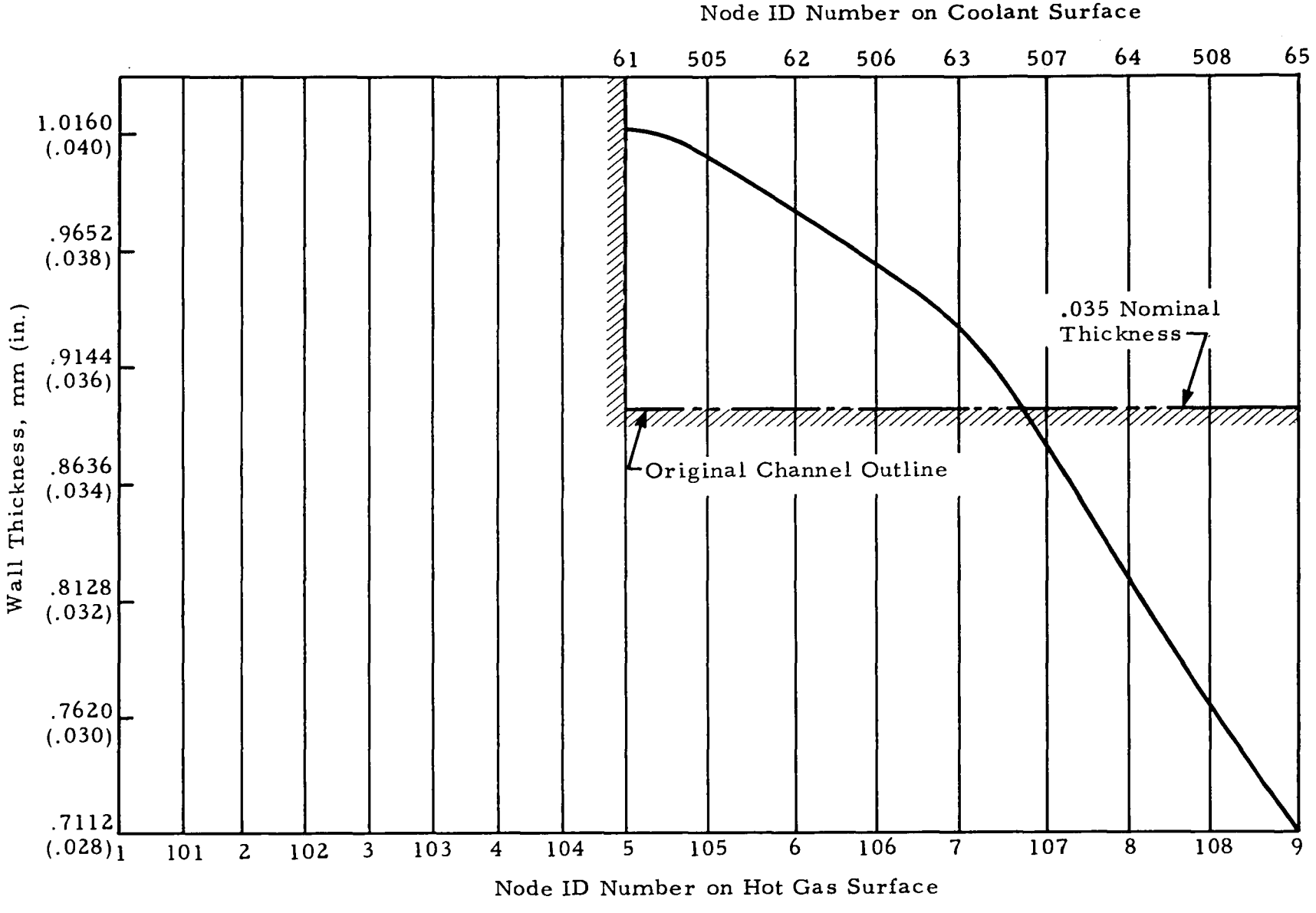

Fig. 23 - Predicted Thickness of Inner Wall Region at End of 200 Cycles on the OFHC Chamber

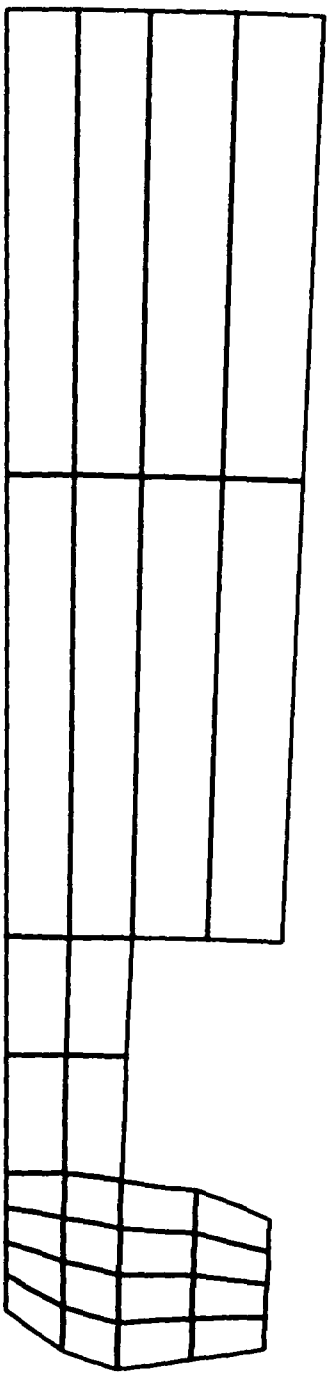

Fig. 24 - Computer Plot of 200-Cycle Configuration of OFHC Chamber

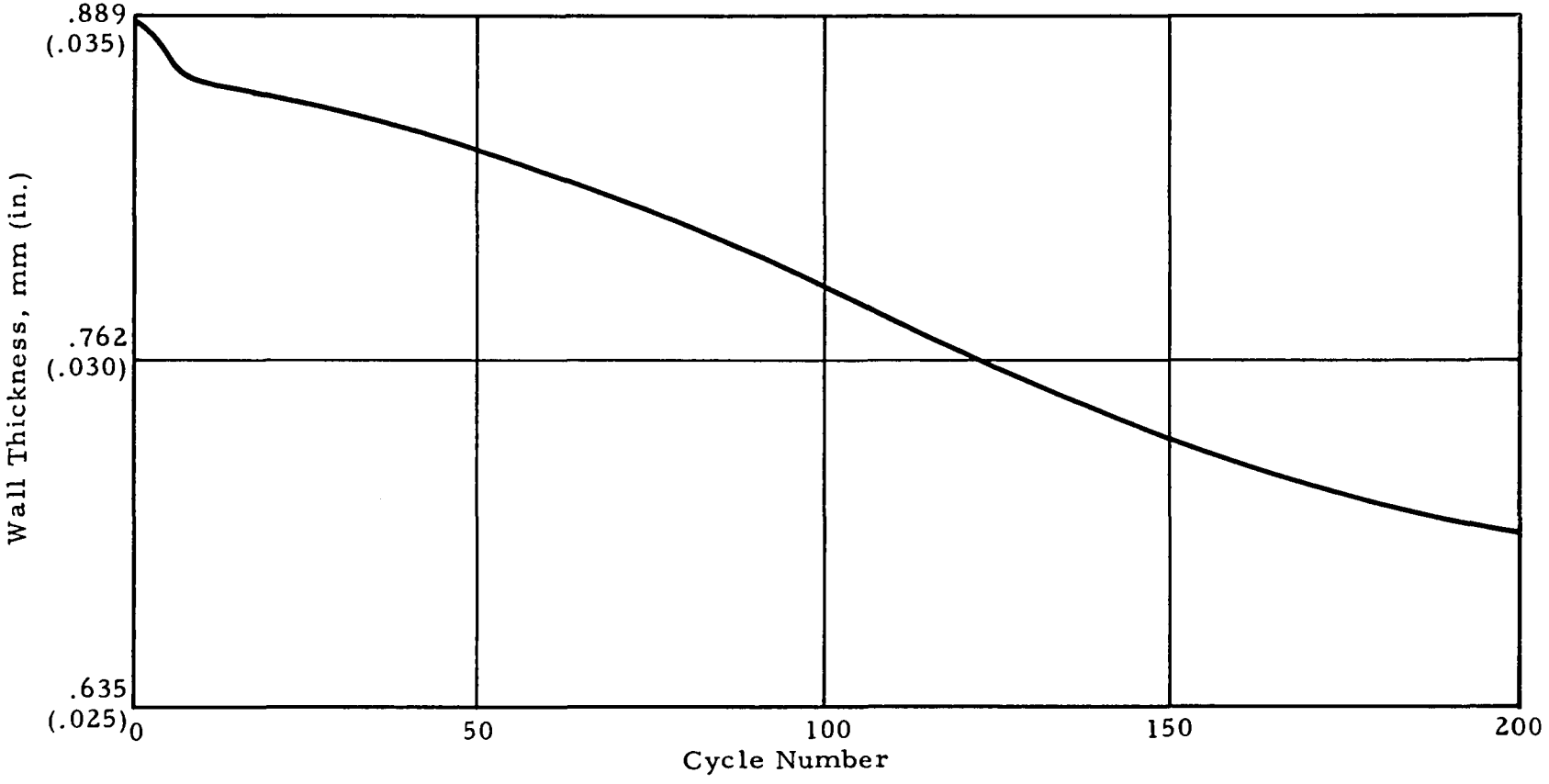

Fig. 25 - OFHC Channel Wall Thickness at Channel Centerline

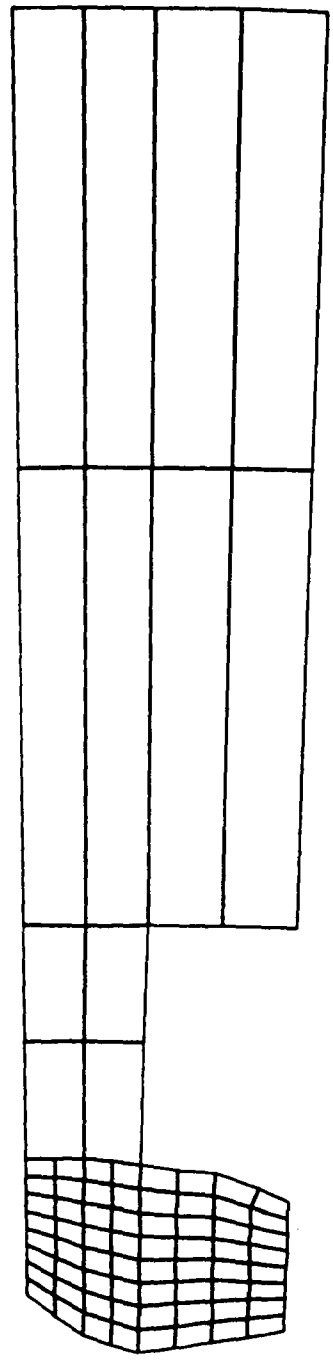

Total Nodes = 104

Total DOF = 208

Total Elements = 76

Fig. 26 - Computer Plot of Model Used for 200-Cycle Configuration Stress Analysis

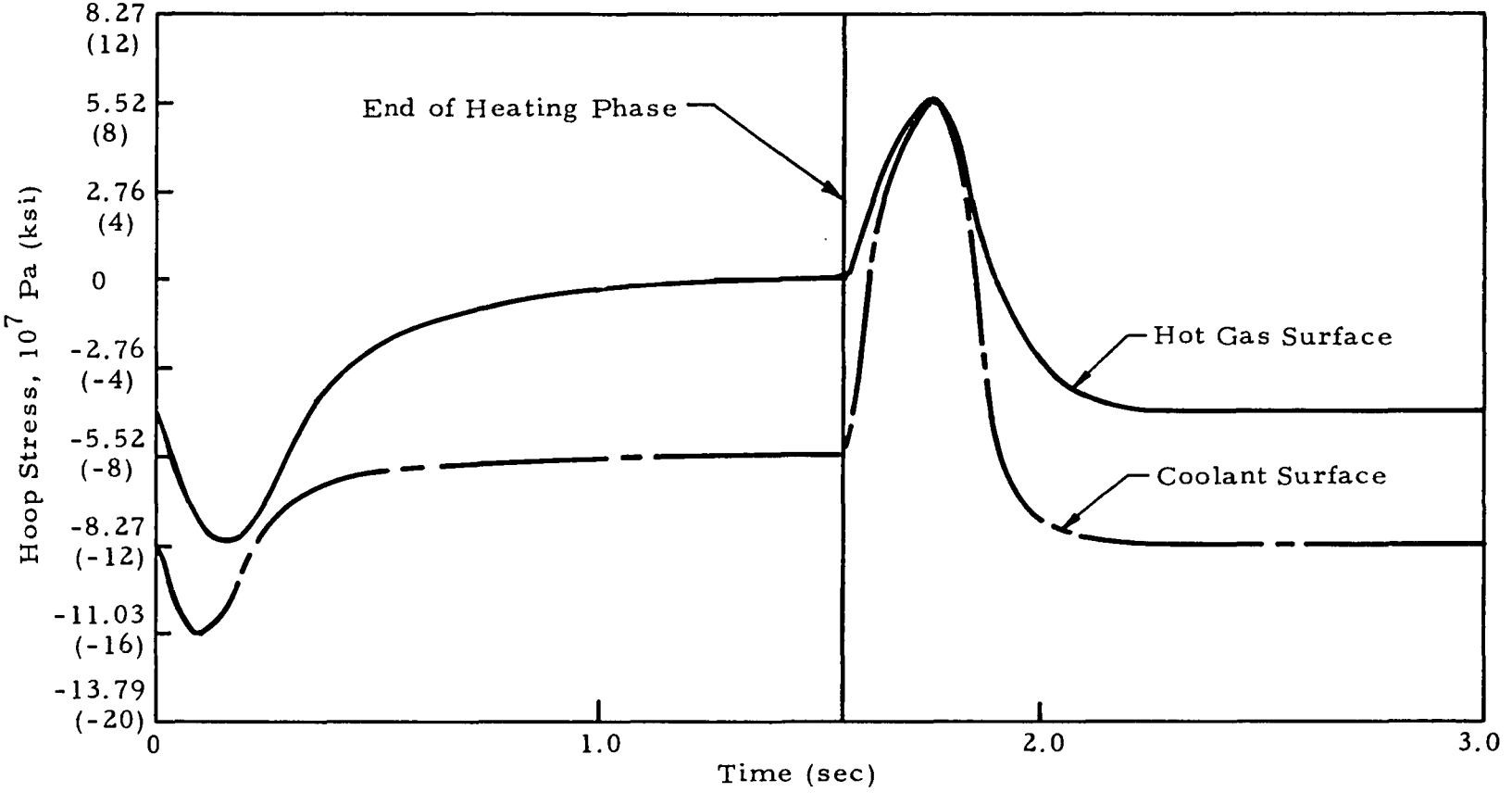

Fig. 27 - Hoop Stress History at Channel Centerline of 200-Cycle Configuration of OFHC Thrust Chamber

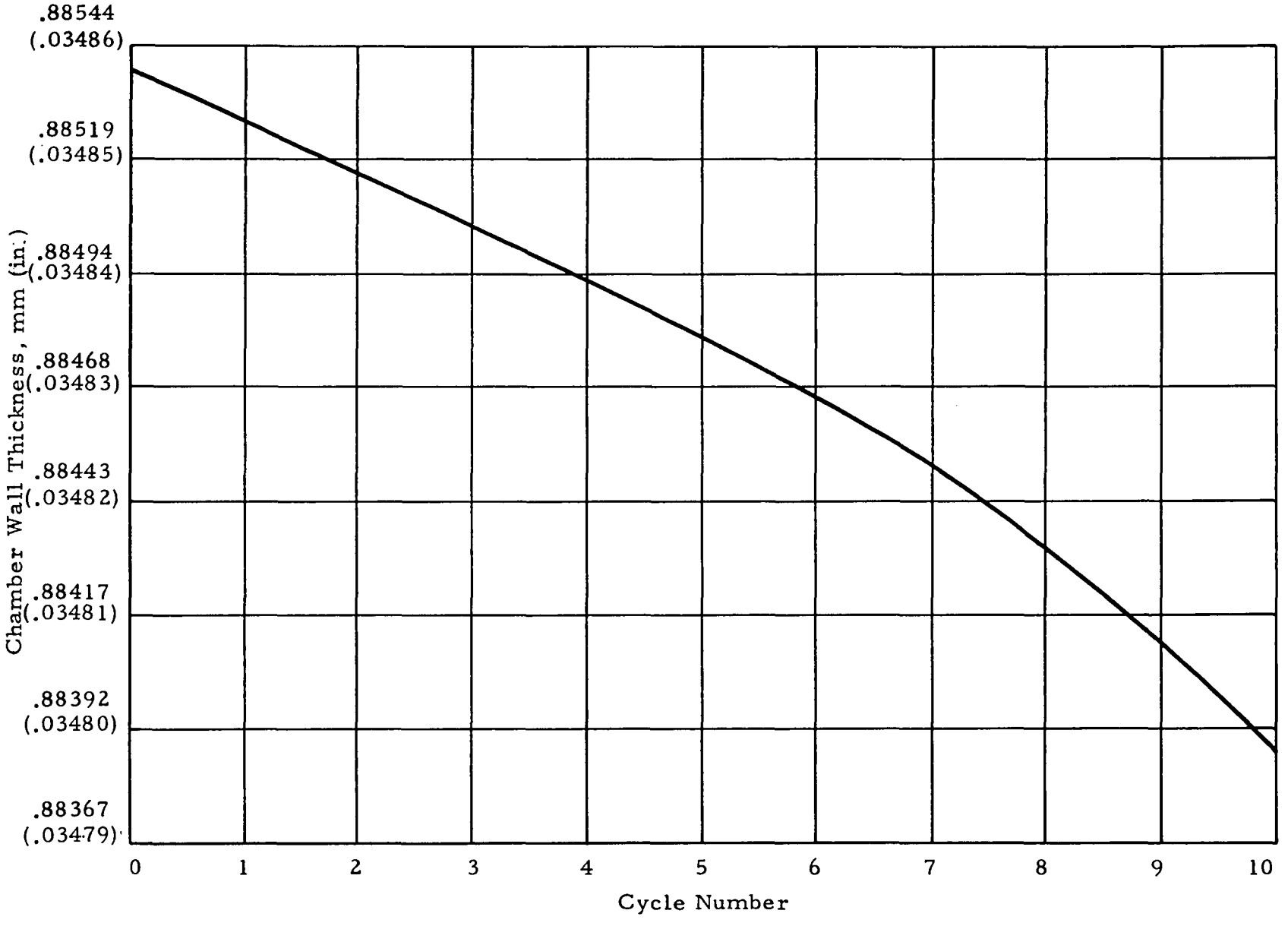

Fig. 28 - Amzirc Chamber Wall Thickness at Centerline of Coolant Channel, Baseline Load Cycle

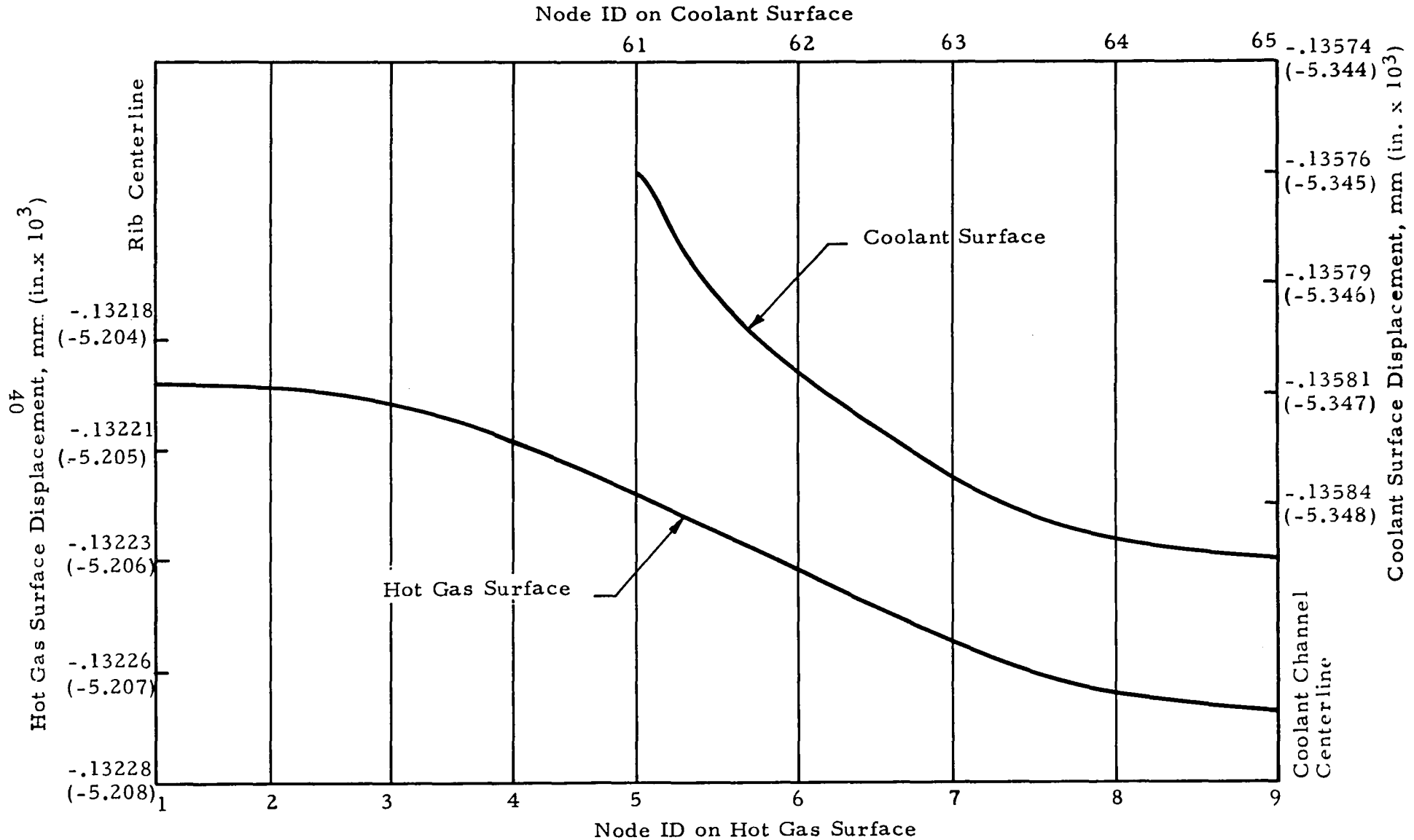

Fig. 29 - Radial Displacement of Hot Gas and Coolant Surface of Amzirc Chamber After Initial Chilldown to Uniform Temperature of 28 K

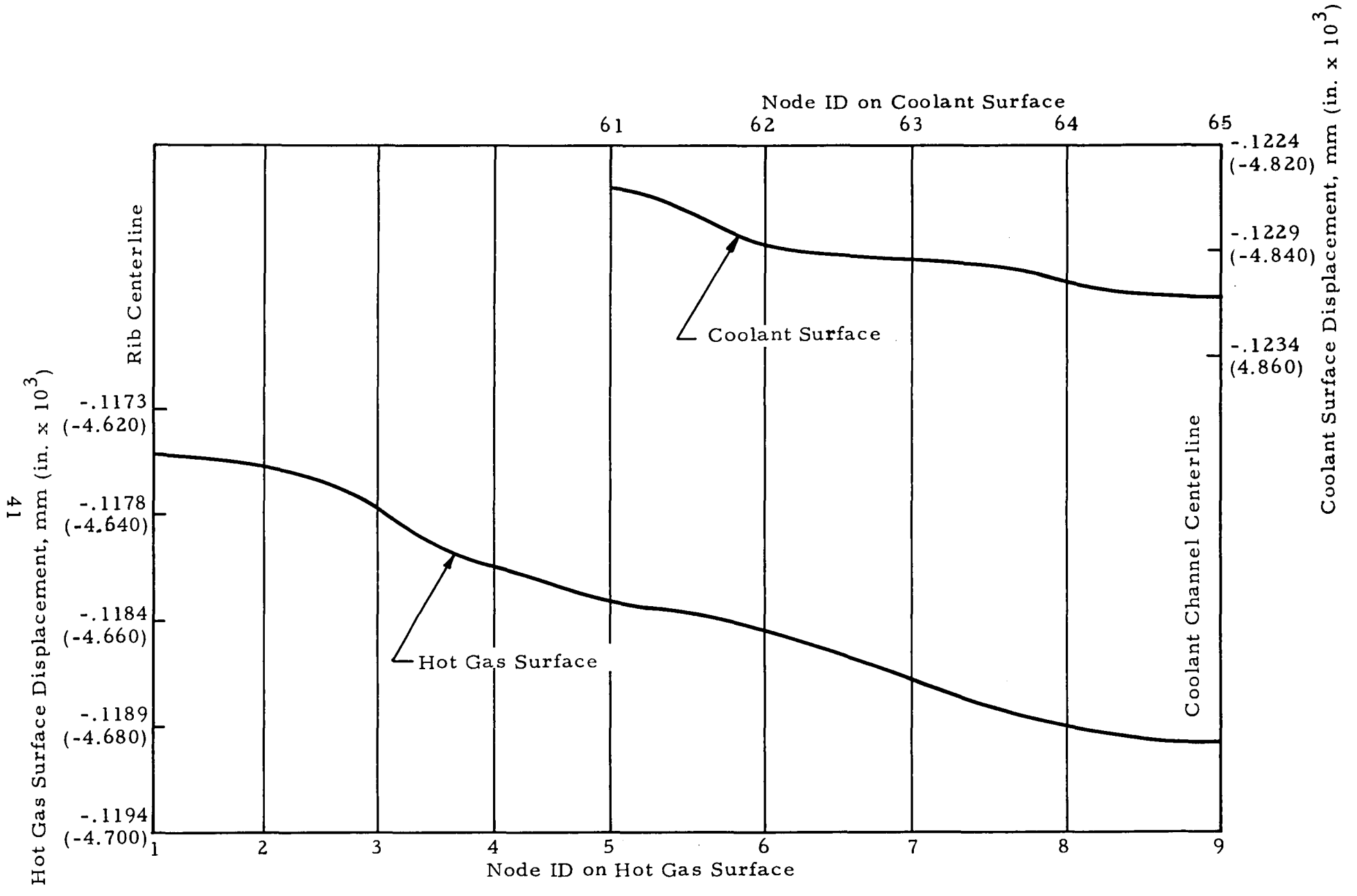

Fig. 30 - Radial Displacement of Hot Gas and Coolant Surfaces of Amzirc Chamber at End of Baseline Temperature Cycle 5

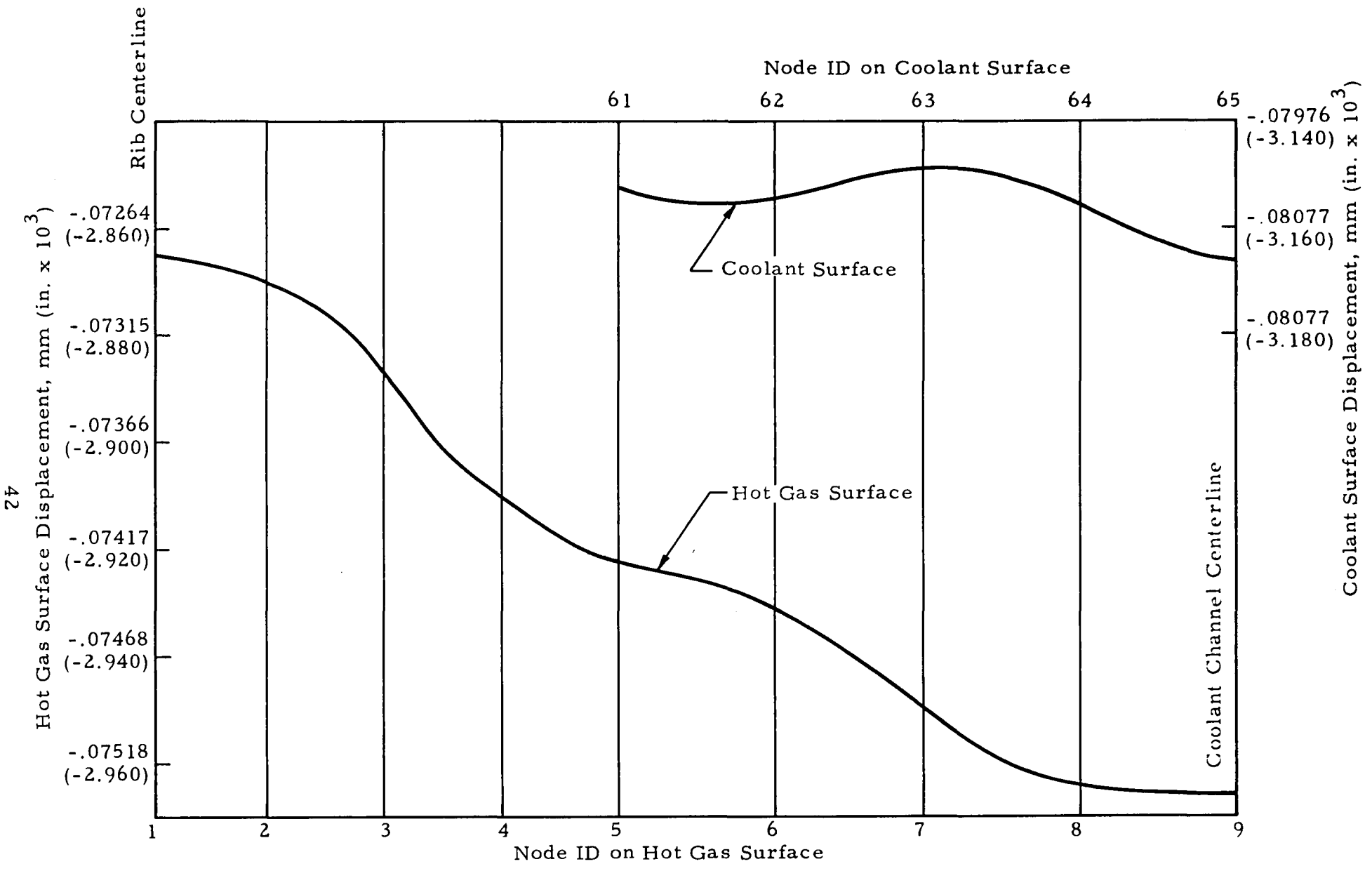

Fig. 31 - Radial Displacement of Hot Gas and Coolant Surfaces of Amzirc Chamber at End of Baseline Temperature Cycle 10

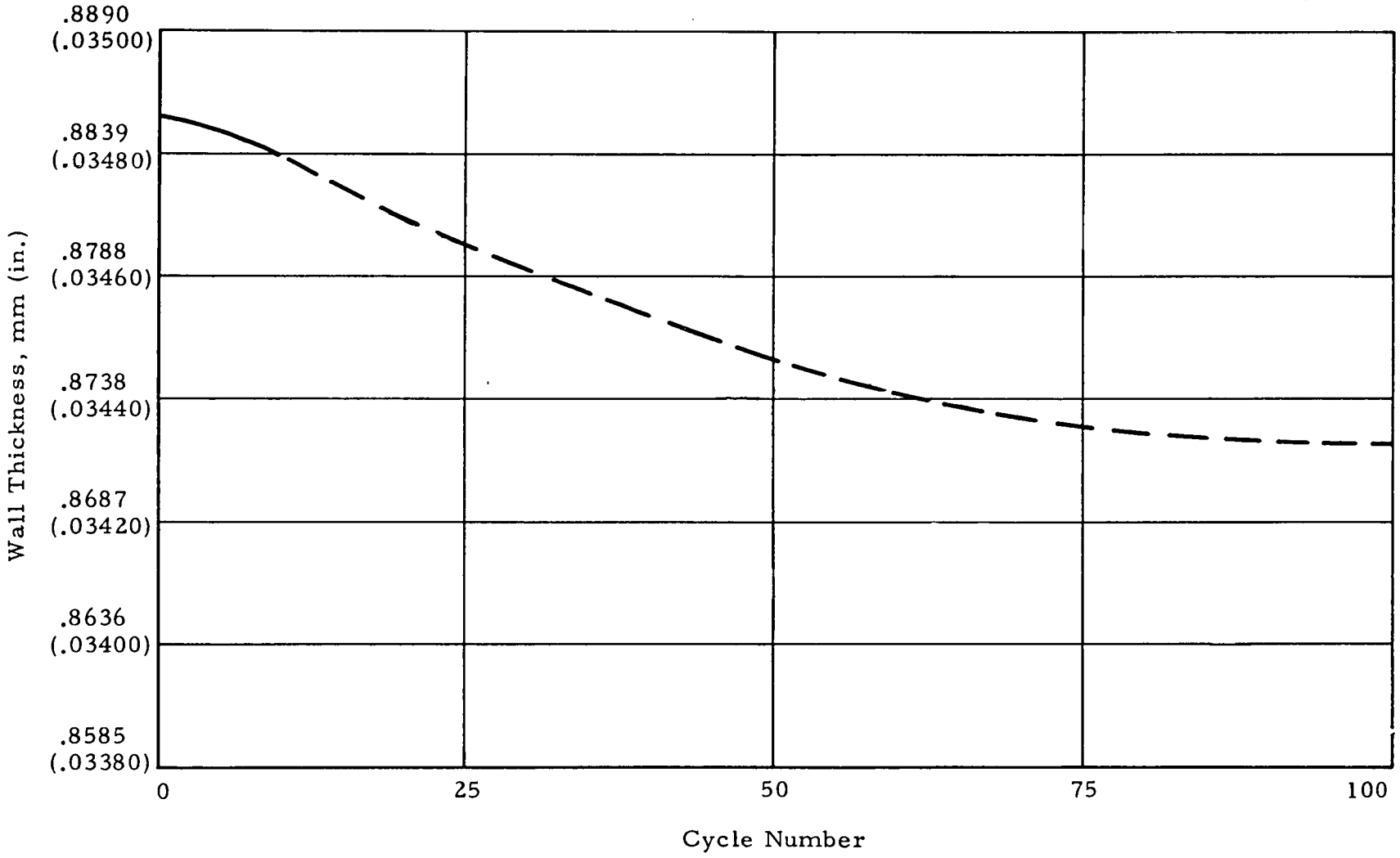

Fig. 32 - Amzirc Chamber Wall Thickness at Centerline of Coolant Channel, Baseline Load Cycle

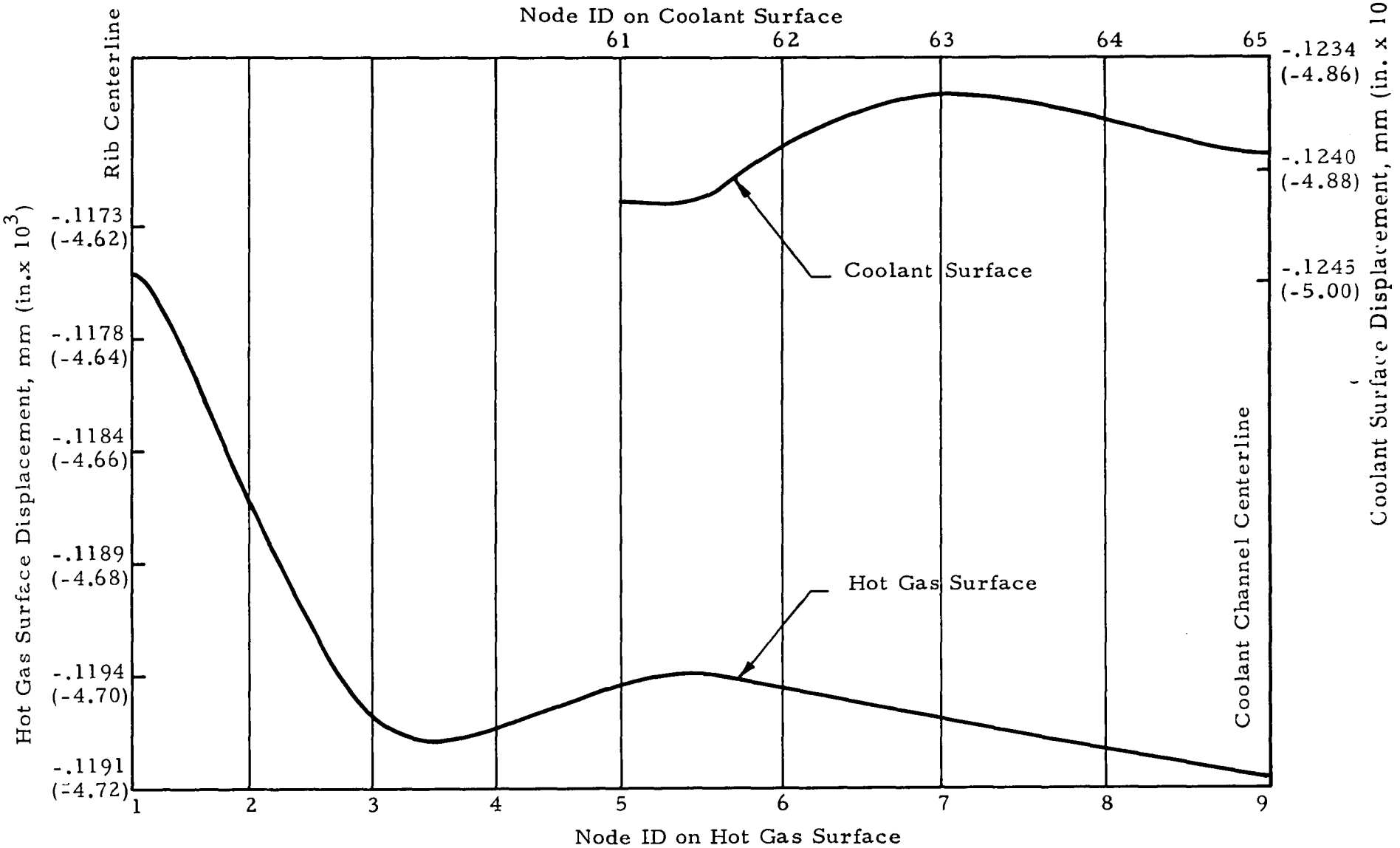

Fig. 33 - Radial Displacement of Hot Gas and Coolant Surfaces of Amzirc Chamber at End High-Temperature Cycle 5

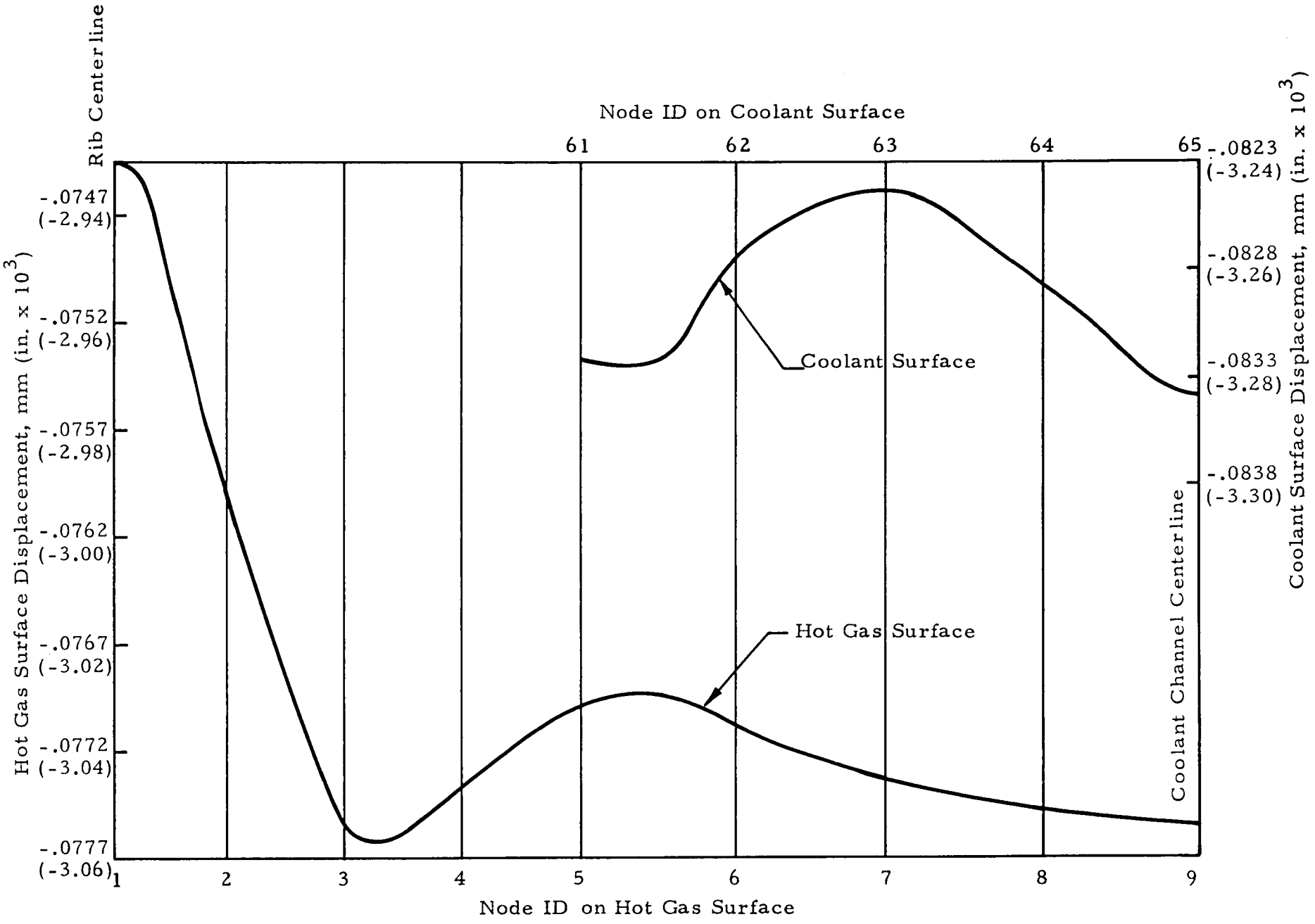

Fig. 34 - Radial Displacement of Hot Gas and Coolant Surfaces of Amzirc Chamber at End of High-Temperature Cycle 10

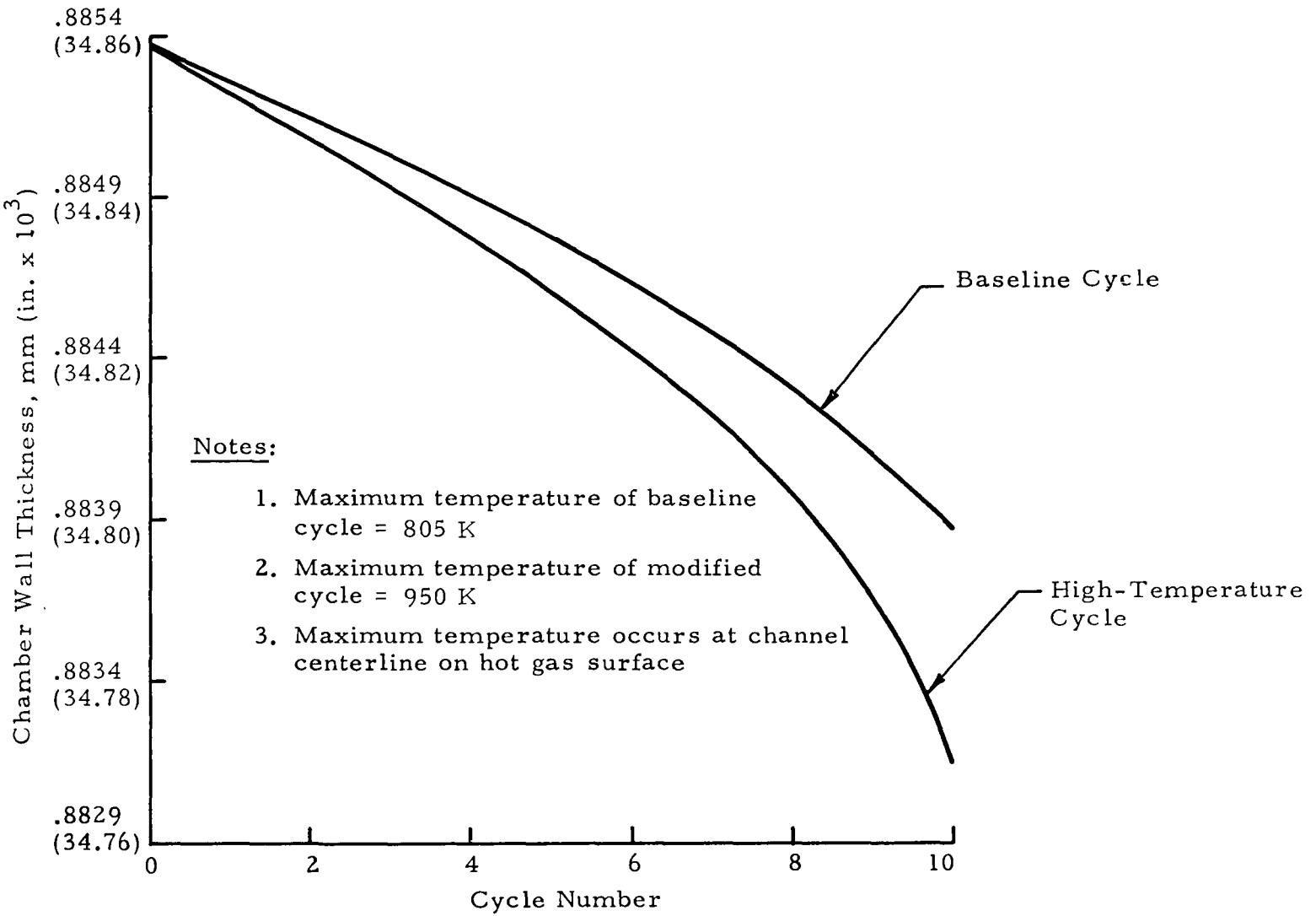

Fig. 35 - Amzirc Chamber Wall Thickness at Centerline of Coolant Channel

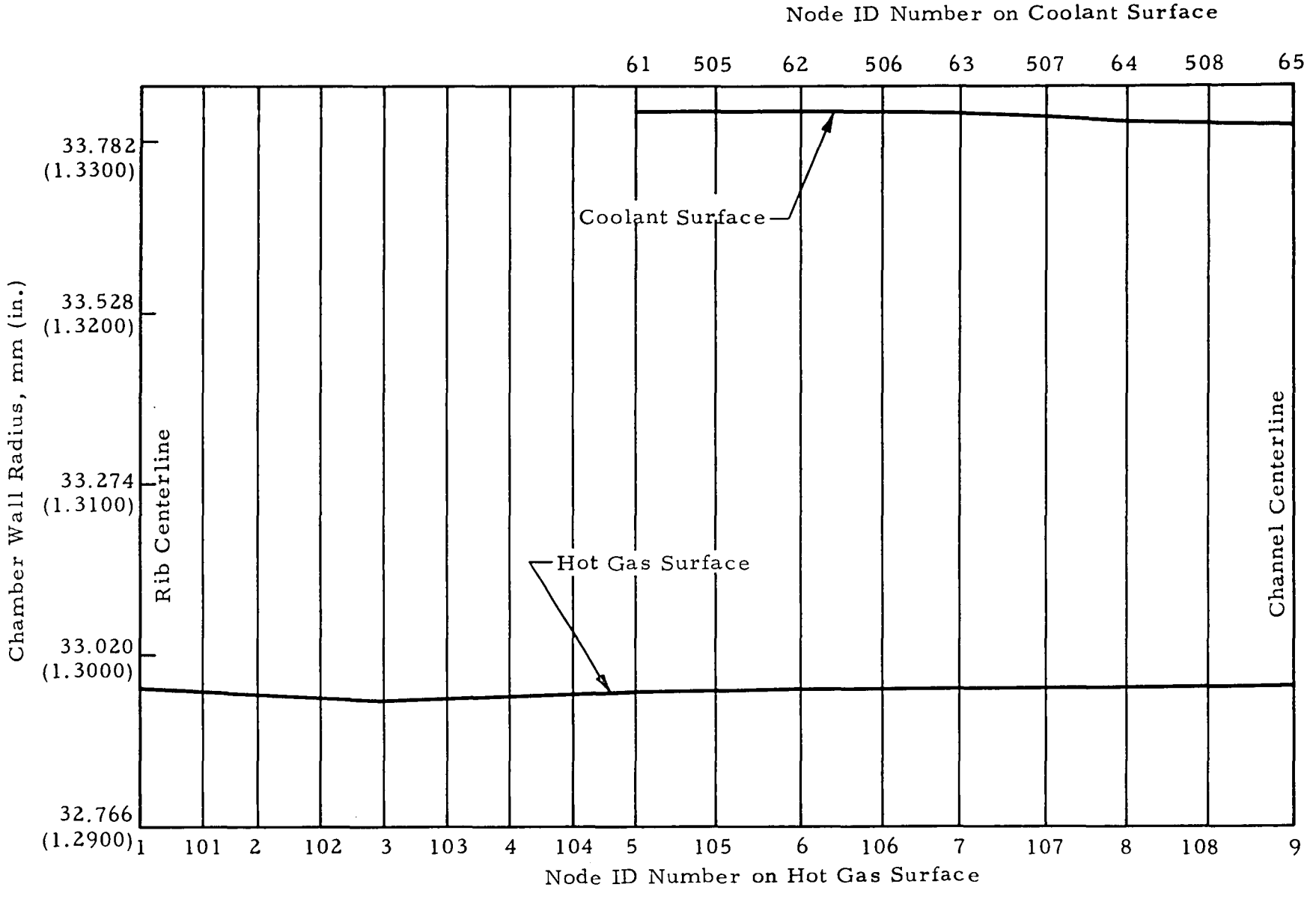

Fig. 36 - Predicted Shape of Inner Wall Region at End of 100 High-Temperature Cycles on the Amzirc Chamber

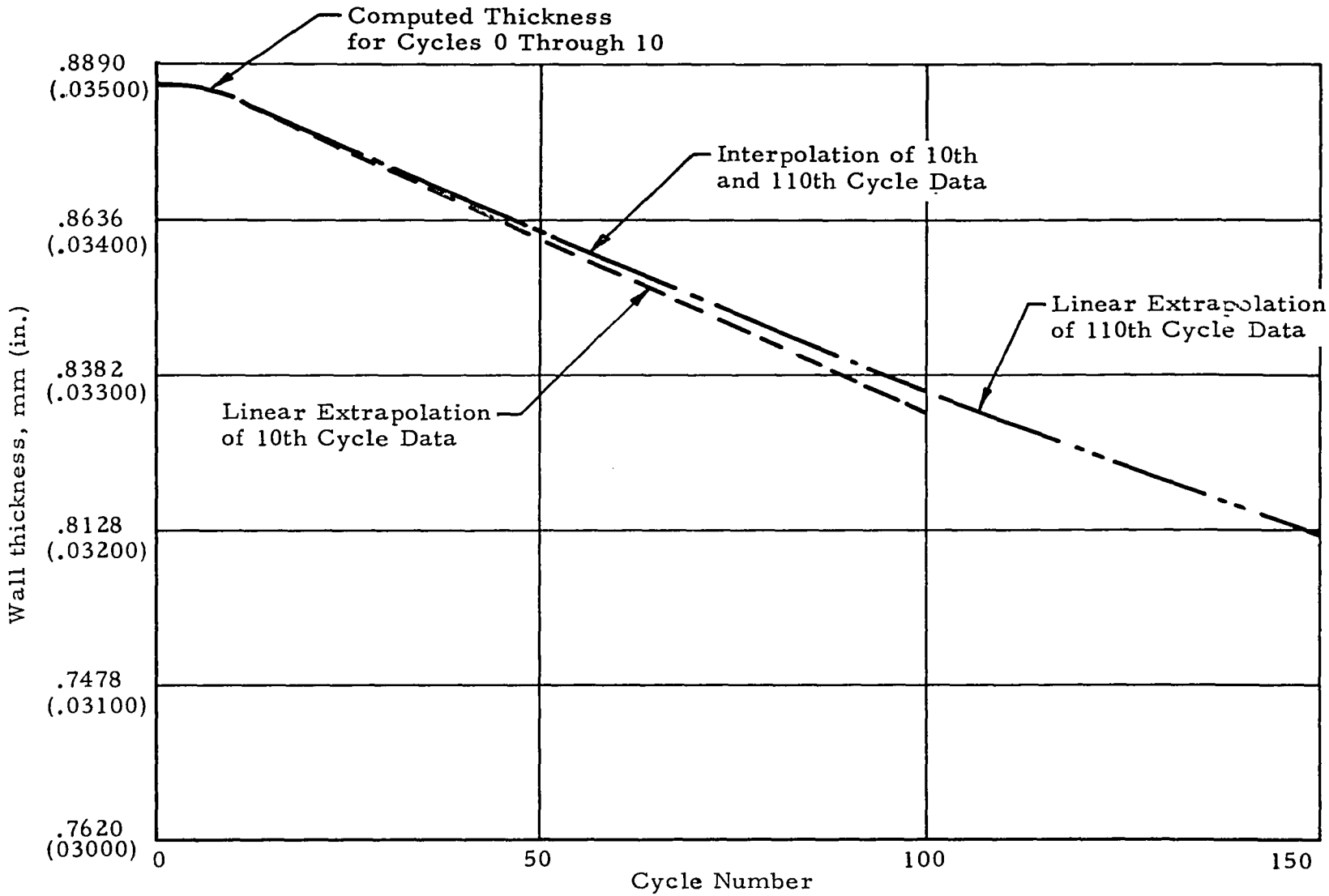

Fig. 37 - Amzirc Channel Wall Thickness at Channel Centerline, High-Temperature Cycle

DISTRIBUTION LIST FOR FINAL REPORT – CR 159522

Name	No. of Copies
National Aeronautics and Space Administration Lewis Research Center 21000 BrookPark Rd. Cleveland, OH 44135	
Attn: Contracting Officer, MS 500-213	1
Technical Utilization Office, MS 7-3	1
Technical Report Control Office, MS 5-5	1
AFSC Liaison Office, MS 501-3	2
Library, MS 60-3	2
Office of Reliability & Quality Assurance, MS 500-211	1
N.T. Musial, MS 500-311	1
H.J. Kasper, Project Manager, MS 501-7	10
E.A. Bourke, MS 501-5	5
National Aeronautics and Space Administration Headquarters Washington, DC 20546	
Attn: Office of Aeronautics & Space Technology	
RS/Director, Manned Space Technology	1
RP/Director, Space Propulsion and Power	1
RW/Director, Materials & Structures	1
RP1/F.W. Stephenson	1
Attn: Office of Manned Space Flight	
MT/Director, Advanced Manned Mission	1
Attn: Office of Space Science	
SG/Director, Physics & Astronomy Programs	1
SL/Director, Planetary Programs	1
SV/Director, Launch Vehicles & Propulsion	1
Attn: Office of Technology Utilization Division	
KT/Director, Technology Utilization	1
National Aeronautics & Space Administration Ames Research Center Moffett Field, CA 94035	
Attn: Library	1
National Aeronautics & Space Administration Flight Research Center P.O. Box 273 Edwards, CA 93523	1

	No. of Copies
National Aeronautics and Space Administration George C. Marshall Space Flight Center Huntsville, AL 35912	
Attn: EP46/R. L. Hurford	1
EH23/W. B. McPherson	1
EP46/N. Schlemmer	1
EP21/J. A. Lombardo	1
EP23/R. H. Counts	1
National Aeronautics and Space Administration Goddard Space Flight Center Greenbelt, MD 20771	
Attn: Library	1
National Aeronautics and Space Administration John F. Kennedy Space Center Cocoa Beach, FL 32931	
Attn: Library	1
National Aeronautics and Space Administration Lyndon B. Johnson Space Center Houston,	
Attn: Library	1
National Aeronautics and Space Administration Langley Research Center Langley Station Hampton, VA 23365	
Attn: Library	1
NASA Scientific & Technical Information Facility P.O. Box 8785 Baltimore-Washington Intn'l. Airport Baltimore, MD 21240	
Attn: Accessioning Department	10
Office of the Director of Defense Research & Engineering Washington, DC 20301	
Attn: Office of Ass't Director (Chem. Technology)	1

	No. of Copies
Jet Propulsion Laboratory 4800 Oak Grove Drive Pasadena, CA 91103	
Attn: Library	1
D. Dipprey	1
Defense Documentation Center Cameron Station, Bldg. 5 5010 Duke St. Alexandria, VA 22314	
Attn: TISIA	1
Advanced Research Projects Agency Washington, DC 20525	
Attn: Library	1
Aeronautical Systems Division Air Force Systems Command Wright-Patterson AFB, OH 45433	
Attn: Library	1
Air Force Rocket Propulsion Laboratory (RPM) Edwards, CA 93523	
Attn: Library	1
Air Force FTC (FTAT-2) Edwards Air Force Base, CA 93523	
Attn: Library	1
Air Force Office of Scientific Research 1400 Wilson Blvd. Arlington, VA 22209	
Attn: Library	1
U.S. Air Force, Office of Information Washington, DC 20333	
Attn: Library	1
Air Force Aero Propulsion Laboratory Research & Technology Division U.S. Air Force Systems Command Wright Patterson AFB, OH 45433	
Attn: Library (APRP)	1

No. of Copies

Arnold Engineering Development Center
Air Force Systems Command
Tullahoma, TN

Attn: Library 1

Bureau of Naval Weapons
Department of the Navy
Washington, DC

Attn: Library 1

U.S. Naval Research Laboratory
Washington, DC 20390

Attn: Library 1

U.S. Army Research Office (Durham)
Box CM, Duke Station
Durham, NC 27706

Attn: Library 1

U.S. Army Missile Command
Redstone Scientific Information Center
Redstone Arsenal, AL 35808

Attn: Document Section 1

U.S. Naval Missile Center
Point Mugu, CA 93041

Attn: Technical Library 1

U.S. Naval Weapons Center
China Lake, CA 93557

Attn: Library 1

Aerojet Liquid Rocket Company
P.O. Box 13222
Sacramento, CA 95813

Attn: Technical Library 1
L. Bassham 1

Aro, Inc.
Arnold Engineering Development Center
Arnold AF Station, TN 37389

Attn: Library 1

No. of Copies

Battelle Memorial Institute
505 King Avenue
Columbus, OH 43201

Attn: Library 1

Bell Aerosystems Inc.
Box 1
Buffalo, NY 14240

Attn: Library 1

Boeing Company, Space Division
P.O. Box 868
Seattle, WA 98124

Attn: Library 1
R.G. Voss 1

Chemical Propulsion Information Agency
Applied Physics Laboratory
8621 Georgia Avenue
Silver Spring, MD 20910 1

Chrysler Corporation
Space Division
P.O. Box 29200
New Orleans, LA 70129

Attn: Library 1

General Electric Company
Missiles & Space Systems Center
Valley Forge Space Tech. Center
P.O. Box 8555
Philadelphia, PA 19101

Attn: Library 1

Grumman Aircraft Engineering Corp.
Bethpage, L.I., NY 11714

Attn: Library 1

Ling-Temco-Vought Corporation
P.O. Box 5907
Dallas, TX 75222

Attn: Library 1

No. of Copies

Lockheed Missiles & Space Company
P.O. Box 504
Sunnyvale, CA 93087

Attn: Library 1

Marquardt Corporation
16555 Staticoy Street
Box 2013 South Annex
Van Nuys, CA 91409

Attn: Library 1

Martin-Marietta Corp.
P.O. Box 179
Denver, CO 80201

Attn: Library 1

McDonnell Douglas Astronautics
5301 Bolsa Avenue
Huntington Beach, CA 92647

Attn: Library 1

Philco-Ford Corp.
Aeronautics Div.
Ford Rd.
Newport Beach, CA 92663

Attn: Library 1

Purdue University
Lafayette, IN 47907

Attn: Library 1

Rocketdyne
A Div. of Rockwell Corp.
6633 Canoga Avenue
Canoga Park, CA 91304

Attn: Library 1
N. Bergstresser 1

Rocket Research Corp.
Willow Road at 116th Street
Redmond, WA 98052

Attn: Library 1

No. of Copies

Thiokol Chemical Corp.
P.O. Box 1000
Newton, PA 18940 — 1

TRW Systems, Inc.
1 Space Park
Redondo Beach, CA 90278

Attn: Library — 1

United Aircraft Corporation
Pratt & Whitney Division
Florida Research & Development Center
P.O. Box 2691
West Palm Beach, FL 33402

Attn: Library — 1

Amax Copper, Inc.
1270 Ave. of the Americas
New York, NY 10020

Attn: N. Kehl — 1
G.C. Van Tilburg — 1

Glidden-Durkee
Metals Group
900 Union Commerce Bldg.
Cleveland, OH 44115

Attn: M.F. Marchitto — 1